Castañeda, I.S., Schouten, S., Paetzold, J., Lucassen, F., Kasemann, S., Kuhlmann, H. & Schefuß, E. (2016). Hydroclimate variability in the Nile River Basin during the past 28,000 years. *Earth and Planetary Science Letters*, 438, 47-56

Published version: dx.doi.org/10.1016/j.epsl.2015.12.014

Hydroclimate variability in the Nile River Basin during the past 28,000 years

Isla S. Castañeda[a,b,1], Stefan Schouten[a], Jürgen Pätzold[c], Friedrich Lucassen[c,d], Simone Kasemann[c,d], Holger Kuhlmann[d], Enno Schefuß[d]

[a]*Department of Marine Organic Biogeochemistry, NIOZ Royal Netherlands Institute for Sea Research, PO Box 59, 1790 AB Den Burg, Netherlands*

[b]*Department of Geosciences, University of Massachusetts Amherst, 233 Morrill Science Center, 611 North Pleasant St., Amherst, MA 01002, USA*

[c]*Faculty of Geosciences, University of Bremen, Klagenfurter Strasse, 28359 Bremen, Germany*

[d]*MARUM Center for Marine Environmental Sciences, University of Bremen, Leobener Strasse, D-28359, Bremen, Germany*

Abstract

It has long been known that extreme changes in North African hydroclimate occurred during the late Pleistocene yet many discrepancies exist between sites regarding the timing, duration and abruptness of events such as Heinrich Stadial (HS) 1 and the African Humid Period (AHP). The hydroclimate history of the Nile River is of particular interest due to its lengthy human occupation history yet there are presently few continuous archives from the Nile River corridor, and pre-Holocene studies are rare. Here we present new organic and inorganic geochemical records of Nile Basin hydroclimate from an eastern Mediterranean (EM) Sea sediment core spanning the past 28 ka BP. Our multi-proxy records reflect the fluctuating inputs of Blue Nile versus White Nile material to the EM Sea in response to gradual changes in local insolation and also capture abrupt hydroclimate events driven by remote climate forcings, such as HS1. We find strong evidence for extreme aridity within the Nile Basin evolving in two distinct phases during HS1, from 17.5 to 16 ka BP and from 16-14.5 ka BP, whereas peak wet conditions during the AHP are observed from 9-7 ka BP. We find that zonal movements of the Congo Air Boundary (CAB), and associated shifts in the dominant moisture source (Atlantic versus Indian Ocean moisture) to the Nile Basin, likely contributed to abrupt hydroclimate variability in northern East Africa during HS1 and the AHP as well as to non-linear behavior of hydroclimate proxies. We note that different proxies show variable gradual and abrupt responses to individual hydroclimate events, and thus might have different inherent sensitivities, which may be a factor partially contributing to the controversy surrounding the abruptness of past events such as the AHP. During the Late Pleistocene the Nile Basin experienced extreme hydroclimate fluctuations, which presumably impacted Paleolithic cultures residing along the Nile corridor.

Keywords: African Humid Period, hydroclimate, Nile River, Heinrich Stadial, leaf wax, deuterium isotopes

1. Introduction

The paleoclimate history of the Nile River valley in East Africa is of interest due to its rich history of human occupation (*Vermeersch and Van Neer*, 2015). Relationships between climate and the distribution of settlements on the Nile River corridor have long been recognized and it is hypothesized that extreme changes in African hydroclimate helped shape the growth and led to the decline of numerous complex societies [*Kuper and*

Kröpelin, 2006]. One of the most dramatic changes in North African hydroclimate, the so-called African Humid Period (AHP) [*deMenocal et al.*, 2000], occurred during the early Holocene when increased rainfall allowed vegetation, lakes and human populations to occupy a "green Sahara", a region that today is a hyperarid desert [*Kuper and Kröpelin*, 2006]. Variability in Nile River flow also played an important role in shaping Egypt's civilizations with the collapse of the Old Kingdom at 4,160 years before present, attributed to a 30 year absence of annual Nile flooding [*Stanley et al.*, 2003]. Although lacking direct evidence, it is hypothesized that HS1, which is recognized as an extreme and widespread drought in North Africa, also had a major impact on Paleolithic cultures [*Stager et al.*, 2011].

Previous investigations of North African hydroclimate since the Last Glacial Maximum (LGM) have documented abrupt and extreme hydrological fluctuations as well as considerable temporal and spatial heterogeneity. The timing and duration of the AHP varies with latitude [e.g. *Kuper and Kröpelin*, 2006] with sites in the north experiencing a shorter humid phase and earlier termination than sites in the south [*Shanahan et al.*, 2015], following changes in northern hemisphere summer insolation. However, whether the transitions leading into and out of the AHP were abrupt, gradual or stepwise (Fig. 1) remains a highly debated issue [e.g. *Kuper and Kröpelin*, 2006; *Costa et al.*, 2014; *deMenocal et al.*, 2000; *Kuhlmann et al.*, 2004; *Schefuß et al.*, 2005; *Tierney and deMenocal*, 2013; *Tierney et al.*, 2008; *McGee et al.*, 2013; *Junginger et al.*, 2014; *Weldeab et al.*, 2014; *Marshall et al.*, 2011; *Kutzbach and Street-Perrott*, 1985; *Claussen et al.*, 1999]. In East Africa, the role of non-linear biogeophysical climate feedbacks is also debated with recent studies concluding that non-linear biogeophysical climate feedbacks between precipitation and vegetation are absent [*Weldeab et al.*, 2014], that a nonlinear convection feedback associated with Indian Ocean SST could be an important contributor to rainfall variability [*Tierney and deMenocal*, 2013], or that a non-linear change in vegetation and sediment erosion occurred in the Early Holocene without a significant decrease in precipitation [*Blanchet et al.*, 2014].

Presently, a gap in our understanding of North African hydroclimate stems from a lack of continuous archives in the vast Nile River corridor [*Bard*, 2013], which spans 35 degrees of latitude (4˚S to 31˚N) over its ca. 6670 km course and has a catchment of nearly 3 million km^2. Here, we investigate the spatially integrated temperature and hydroclimate history of the Nile River Basin by examining the geochemistry of a sediment core collected from the Eastern Mediterranean (EM) Sea that receives sediment from the Nile River. We measured multiple organic and inorganic geochemical parameters on the same samples to provide a robust assessment of past hydroclimate variability and to examine shifts in the dominant sources of material transported by the Nile River to the EM Sea. We focus the discussion on two extreme and contrasting hydroclimate events: Heinrich Stadial (HS) 1, an arid interval driven by an abrupt external forcing, and the AHP, a wet period driven by gradual changes in insolation. We note that the term abrupt is used qualitatively in many paleoclimate studies; for the purpose of this study we consider an event as abrupt if its onset or termination occurs in 1,000 years or less.

2. Study Location

Sediment core GeoB7702-3 was collected from the continental slope offshore Israel (31˚39.1'N, 34˚04.4'E, 562 m water depth) during R/V Meteor cruise M52/2 in 2002 (Fig.

2) [*Pätzold et al.*, 2003]. The chronology of this 592 cm long core, which spans the past 28,000 years before present (hereafter 28 ka BP), is based on 15 AMS ^{14}C dates on foraminifera and was previously published along with alkenone and TEX_{86} sea surface temperature (SST) estimates [*Castañeda et al.*, 2010]. The surface currents flow in an anticlockwise direction around the basin and sediment from the Nile River is transported eastward to the coring site [*Weldeab et al.*, 2002].

Precipitation over the Nile Basin derives from both Atlantic and Indian Ocean sources [*Gimeno et al.*, 2010]. Total annual precipitation within the Nile Basin fluctuates widely (Fig. 2) related to the varying geographical influence of the Intertropical Convergence Zone (ITCZ), marking the convergence of the northeast and southwest trade winds, and the Congo Air Boundary (CAB), separating Atlantic and Indian Ocean sourced moisture [*Camberlin*, 2009] (Fig. 1). In boreal summer when the ITCZ is at its northernmost position, the CAB is at its most northerly and easterly extent, drawing Atlantic moisture to East Africa. Conversely, when the ITCZ is at its southernmost position in boreal winter, the CAB is located further to the south and does not extend as far eastward, restricting the flow of Atlantic moisture across the continent [*Camberlin*, 2009]. From north to south within the Nile Basin, the length of the rainy season increases as does the total rainfall amount [*Camberlin*, 2009] (Fig. 2c).

3. Methods

3.1. Organic geochemical analyses

Core GeoB7702-3 was sampled at 5 cm intervals (average time step of 209 years) for organic geochemical analyses using the methods detailed by *Castañeda et al.* [2010].

Freeze dried sediment samples were extracted with 9:1 dichloromethane (DCM)/methanol (v/v) using an Accelerated Solvent Extractor (ASE 200). Alumina oxide column chromatography was used to separate apolar, ketone and polar fractions with solvent mixtures of 9:1 hexane/DCM (v/v), 1:1 hexane/DCM (v/v), and 1:1 DCM/methanol (v/v), respectively. The apolar fractions were separated into saturated and unsaturated hydrocarbon fractions using $AgNO_3$-impregnated silica gel. The saturated fractions were analyzed at MARUM, University of Bremen. A Thermo Trace gas chromatograph (GC) coupled via a combustion reactor to a MAT252 mass spectrometer (MS) was used to measure the carbon isotopic composition ($\delta^{13}C$) of *n*-alkanes while a Thermo Trace GC coupled to a MAT253 MS was used to determine their deterium (δD) isotopic composition. Isotope values were measured against calibrated reference gas using H_2 for δD and CO_2 for $\delta^{13}C$. δD and $\delta^{13}C$ values are reported in ‰ versus VSMOW and VPDB, respectively. The performance of the systems was checked every sixth analyses by measurement of an *n*-alkane standard containing 16 compounds ranging from -33‰ to -261‰ VSMOW. Measurements were only conducted when average absolute deviations against offline values were <0.3‰ and <3‰ for $\delta^{13}C$ and δD, respectively. The H_3^+-factor was monitored daily and was constant at 5.34 ±0.03‰ (n=28) for the measuring time. Further information is provided by *Schefuß et al.* [2011]. We measured $\delta^{13}C$ and δD on the C_{31} *n*-alkane, the most abundant homologue. Reproducibility (the standard deviations of multiple analyses) varied between 0‰ and 0.5‰ (average 0.1‰) for $\delta^{13}C$, and 0‰ and 4‰ (average 1‰) for δD. Leaf wax δD values were corrected for global ice volume changes using the method described by *Wang et al.* [2013].

Glycerol dialkyl glycerol tetraethers (GDGTs) were analyzed at NIOZ Royal Netherlands Institute for Sea Research using the methods described by *Castañeda et al.* [2010]. We previously examined EM SST using TEX_{86} [*Castañeda et al.*, 2010]. Here the newer BAYSPAR calibration [*Tierney and Tingley*, 2014] is applied to the TEX_{86} record. The deep water (>1000 m) Mediterranean Sea TEX_{86} calibration of *Kim et al.* [2015] yields approximately 4°C lower temperatures throughout the Holocene but overall trends remain the same. We additionally analyzed branched GDGTs to examine the MBT' and CBT indices [*Weijers et al.*, 2007; *Peterse et al.*, 2012], proxies for mean annual air temperature (MAAT) and soil pH.

3.2. Radiogenic Isotopes

Strontium (Sr) and neodymium (Nd) isotope ratios of bulk sediment samples were analyzed by thermal ionization mass spectrometry (TIMS) on a Thermo Scientific Triton Plus instrument at the Isotope Geochemistry Laboratory at MARUM. Homogenized sediment powders were washed in 18.2 mΩ water and approximately 100 mg were dissolved in a 5:1 mixture of triple distilled HF and HNO_3, dried, and re-dissolved in 1000l of 2 molar HNO_3 for chemical separation.

Sr was isolated from the matrix elements using miniaturized columns with 70 L Sr.Spec resin (Eichrom Technologies, LLC, USA) following a separation procedure adapted from *Deniel and Pin* [2001]. Rare earth elements (REE) were isolated as group from the run-off of the Sr separation by TRU.Spec resin followed by the isolation of Nd from Sm by LN.Spec resin. The setup of the REE and Nd separation columns and separation scheme was adapted from *Pin et al.* [1994] and *Mikova and Denkova* [2007]. Total procedure blanks of Sr and Nd were below 140 pg and 80 pg, respectively, insignificant with respect to the amount of sample material used for analyses.

Sr was loaded with Ta-oxide emitter on Re single filaments and Nd with 0.1m phosphoric acid on a Re double filament configuration and analyzed by TIMS in static multi-collection mode. Instrumental mass-fractionation of Sr and Nd isotope ratios was normalized to $^{87}Sr/^{86}Sr$ of 0.1194 and $^{143}Nd/^{144}Nd$ of 0.7219, respectively. The external long-term reproducibility according to the NIST 987 standard material is $^{87}Sr/^{86}Sr$ 0.710256±16 (2SD, n=33; period: January 2013 to April 2014), according to Nd standard material JNdi–1 $^{143}Nd/^{144}Nd$ is 0.512104±14 (2SD, n=23; period: December 2011 to June 2014).

3.3. XRF core scanning

Element intensities were collected every 1 cm over a 12 mm^2 area with down-core slit size of 10 mm using generator settings of 10 kV, a current of 200 mA, and a sampling time of 30 seconds directly at the split core surface of the archive half with XRF Core Scanner II (AVAATECH Serial No. 2) at the MARUM. The split core surface was covered with a 3 m thin SPEXCerti Prep Ultralene 1 foil. The data reported here were acquired by an Amptek XR-100CR detector, the Amptek Digital Spectrum Analyzer PX2T/CR Power Supply/Shaper and Amplifier, and an Oxford Instruments XTF5011 X-Ray Tube 93057 with rhodium (Rh) target material. Raw data spectra were processed by the analysis of X-ray spectra by Iterative Least square software (WIN AXIL) package from Canberra Eurisys.

3.4. Magnetic susceptibility (Multi-Sensor Core logger)

Magnetic susceptibility (MS) was acquired non-destructively using a GEOTEK™ (Surrey, UK) Multi-Sensor Core Logger (MSCL) at the MARUM. The measurements were made in 1 cm steps over an area of 1 cm^2 using the BARTINGTON™ point-sensor MS2F. The resulting data is the volume specific MS in e^{-5} SI units.

4. Results and Discussion

4.1. Sources of material to the coring site

Due to its large size, the presence of multiple vegetation zones and contrasting environmental conditions within the Nile Basin, a first step to interpreting the GeoB7702-3 proxy records was to determine the main sources of terrestrial material to the core site. The Nile River is comprised of two major tributaries, the White Nile and the Blue/Atbara Nile, which drain contrasting geologic terranes and climate zones [*Krom et al.*, 2002]. The Blue Nile, sourced at Lake Tana, and the Atbara, drain catchments in the Ethiopian Highlands largely consisting of Cenozoic volcanic rocks with low $^{87}Sr/^{86}Sr$ values (0.7030 to 0.7048) and high εNd values [*Krom et al.*, 2002; *Box et al.*, 2011; *Blanchet et al.*, 2013; *Blanchet et al.*, 2014]. In contrast, the White Nile is sourced at equatorial Lake Victoria and the Precambrian crystalline basement rocks in its catchment are characterized by a higher $^{87}Sr/^{86}Sr$ values (approximately 0.7105) and low εNd values [*Krom et al.*, 2002; *Box et al.*, 2011; *Blanchet et al.*, 2013; *Blanchet et al.*, 2014]. Saharan dust is characterized by high $^{87}Sr/^{86}Sr$ values of >0.7173 [*Krom et al.*, 2002; *Weldeab et al.*, 2002] while loess sequences of the Negev desert (southern Israel; Fig. 2b) have $^{87}Sr/^{86}Sr$ values of 0.785 to 0.7114 and εNd values of -11.6 to -4.6 [*Ben Israel et al.*, 2015]. In GeoB7702-3, $^{87}Sr/^{86}Sr$

values range from 0.7080 to 0.7090 and thus likely represent a mixture of material derived from the Blue Nile and White Nile (Fig. 3). These results are in good agreement with those of nearby core 9509 (Fig. 2b) in the EM Sea [*Box et al.*, 2011]. While some locations in the EM Sea receive significant contributions of Saharan dust, the influence of eolian material is minimal near the Nile Delta [*Box et al.*, 2011]. A crossplot of $^{87}Sr/^{86}Sr$ ratios and εNd can further differentiate sources of material from north and east Africa to the EM Sea [*Blanchet et al.*, 2013] and suggests that Saharan dust is not a significant contributor to site GeoB7702-3 (Fig. 3a). We acknowledge that significant contributions of Saharan dust to the core site in the past under different climate regimes cannot be fully ruled out. We also note that loess sequences of the Negev have a similar radiogenic isotopic composition to the White Nile [*Ben Israel et al.*, 2015]. Negev loess derives from the Sinai–Negev dune field, which in turn is sourced from the Nile Delta [*Ben Israel et al.*, 2015; *Amit et al.*, 2011; *Muhs et al.*, 2013]. This material can reach the EM Sea via the Wadi El Arish and although this drainage is quite dry today it may have provided an additional source of material during the AHP [*Muhs et al.*, 2013].

The radiogenic isotope records, which we interpret as mainly reflecting Blue versus White Nile sources, suggest increased input of Blue Nile material from 28 to 16 ka BP followed by a shift to increased input of White Nile material at 14 ka BP (Fig. 3b). A return to increased Blue Nile input occurs at 12 ka BP (the Younger Dryas) and subsequently a dramatic shift to increased contributions of White Nile material occurs, peaking in the early Holocene (Fig. 3b). The mid to late Holocene is characterized by an overall shift to increased inputs of Blue Nile material. These patterns have been previously documented and are attributed to the role of Ethiopian Highland vegetation on Blue Nile sediment supply: during arid climate intervals limited vegetation cover in the Ethiopian Highlands allowed for greater soil erosion during the summer monsoon rainy season whereas during humid periods more extensive vegetation cover reduced erosion and led to relatively larger inputs of White Nile material [*Krom et al.*, 2002; *Box et al.*, 2011].

4.2. Hydroclimate proxies

Long-chain *n*-alkanes form a major component of higher plant epicuticular leaf waxes [*Eglinton and Hamilton*, 1967]. The carbon isotopic composition of plant leaf waxes (hereafter $\delta^{13}C_{wax}$) can be used to distinguish between plants utilizing the C_3 and C_4 photosynthetic pathways [e.g. *Schefuß et al.*, 2003; *Castañeda et al.*, 2009]. For the C_{31} *n*-alkane, C_3 plants (most trees and cool-season grasses and sedges) are characterized by $\delta^{13}C_{wax}$ values of around -35.2‰ while C_4 plants (warm-season grasses and sedges) are more enriched in ^{13}C and have $\delta^{13}C_{wax}$ values of around -21.7‰ [*Castañeda et al.*, 2009]. Aridity is recognized as the dominant control on the large-scale distribution of C_3 versus C_4 vegetation in tropical Africa [*Schefuß et al.*, 2003; *Castañeda et al.*, 2009]. The deuterium isotopic composition of plant leaf waxes (hereafter δD_{wax}) provides information on the isotopic composition of precipitation [e.g. *Schefuß et al.*, 2005]. δD_{wax} has been interpreted to mainly reflect variability in precipitation amount in tropical Africa [e.g. *Schefuß et al.*, 2005; *Tierney et al.*, 2008; *Berke et al.*, 2012; *Tierney and deMenocal, 2013*; *Costa et al.*, 2014; *Shanahan et al.*, 2015] (e.g. the "amount effect") although more generally the isotopic composition of precipitation reflects the overall atmospheric transport history of the airmass from which the moisture is derived (e.g. atmospheric circulation) [*Dansgaard*, 1964; *Risi et al.*, 2008]. As will be discussed in section 4.4, our data suggest that while mainly reflecting rainfall amount, changes in the dominant moisture source also contributed to isotopic variability in Nile Basin δD_{wax}. Leaf waxes are transported by both eolian and fluvial processes but input via the Nile River is the dominant source to GeoB7702-3.

The δD_{wax} record of GeoB7702-3 reveals large changes of approximately 64‰ during the past 28 ka BP (Fig. 4f), with ice volume corrected values ranging from -172‰ to -108‰, suggesting significant hydrological variability in the Nile Basin. While δD_{wax} reflects the isotopic composition of precipitation, additional physiological and environmental factors can modify the isotopic signal including isotopic enrichment under arid conditions from evapotranspiration [*Sachse et al.*, 2012] or soil evaporation [*Schefuß et al.*, 2005; *Sachse et al.*, 2012] as well as isotopic depletion due to increased precipitation amount in monsoon regions [*Risi et al.*, 2008]. Vegetation type also can exert an influence on δD_{wax} values as apparent fractionation varies between plant life-forms, which may either amplify or reduce the signal [*Sachse et al.*, 2012]. In GeoB7702-3, from 11-28 ka BP δD_{wax} and $\delta^{13}C_{wax}$ are strongly positively correlated ($r^2 = 0.56$) but from 11-0 ka BP only a weak correlation exists ($r^2 = 0.19$) suggesting that during the Holocene large fluctuations in δD_{wax} were not driven by changes in vegetation type. Although the δD_{wax} and $\delta^{13}C_{wax}$ track each other prior to the Holocene, given that $\delta^{13}C_{wax}$ values vary by only 1.5‰ in the interval from 11-28 ka BP, vegetation changes were not a main factor driving variability in the δD_{wax} in the older portion of the core (Supplementary Material).

The overall δD_{wax} record suggests arid conditions in the Nile Basin from 28 to 16 ka BP. Within this interval, the highest δD_{wax} values of the entire record are noted during Heinrich Stadials (HS) 2 and 1 (Fig. 4). After HS1, a trend to lower δD_{wax} values occurs until 12 ka BP when a reversal to higher δD_{wax} values denotes the onset of the Younger Dryas. Between 11 and 9.1 ka BP, a dramatic shift of ca. -40‰ occurs, marking the AHP, which is subsequently followed by an overall trend to increasingly higher δD_{wax} values toward the present.

Continental-scale changes in vegetation type in tropical Africa are mainly driven by precipitation and thus it might be expected that $\delta^{13}C_{wax}$ should closely track changes in δD_{wax}. Overall trends in δD_{wax} and $\delta^{13}C_{wax}$ are similar in the interval prior to 11 ka BP with increased C_4 inputs noted concurrently with high δD_{wax} values, indicating arid conditions (Fig. 4; Supplementary Material). However, the two proxies diverge in the Holocene when during the AHP a shift to increased contributions of C_4 plants is noted followed by a gradual shift to increased C_3 inputs toward the present. This pattern has previously been observed in the Nile Basin and is attributed to the northward migration of the rain belt during the AHP, which caused the expansion of C_4 vegetation into previously barren regions of the Sahara [*Blanchet et al.*, 2014].

We examined branched GDGTs to reconstruct mean annual air temperature (MAAT) and soil pH within the Nile Basin using the MBT'/CBT [*Peterse et al.*, 2012] and CBT indices [*Weijers et al.*, 2007], respectively (Fig. 4b and h). The CBT Index provides an independent hydroclimate proxy and can be used as a relative indicator of wet versus arid conditions because higher precipitation leads to lower (more acidic) pH values [*Weijers et al.*, 2007]. Overall trends in the CBT-derived soil pH record (Fig. 4h) track the δD_{wax} record (Fig. 4f). However, within the AHP interval, the soil pH record reflects a more gradual onset (starting at ca. 11 ka BP) and termination (at ca. 5.7 ka BP) of maximum wet conditions in comparison to the δD_{wax} record, which indicates an abrupt shift to the most depleted values of the entire record in the early Holocene from ca. 9 to 7 ka BP (section 4.4). Likewise, a gradual onset and termination of the AHP is noted in the MBT'/CBT-derived MAAT record.

Another hydroclimate proxy is provided by elemental data from XRF core scanning, yielding information on past variability in Nile River flow. High iron (Fe) content in the EM Sea is attributed to high Nile flood intensity [*Revel et al.*, 2010]. Likewise, the ratios of titanium (Ti) or iron (Fe) to aluminum (Al) in the EM Sea are attributed to fluctuations in material deriving from the Ethiopian Highlands [*Box et al.*, 2011]. Ti to calcium (Ca) ratios are often used to examine terrigenous versus marine input. In GeoB7702-3 the lowest Fe/Al and Ti/Ca ratios are from ca. 15.7 to 14 ka BP signaling low runoff (Fig. 4a). We note that the Ti/Al and Fe/Ca ratios (not plotted) yield exactly the same trends as the Fe/Al and Ti/Ca records, respectively. At around 17-16 ka BP, Lakes Tana and Victoria, the sources of the Blue and While Nile, desiccated [*Lamb et al.*, 2007; *Stager et al.*, 2011]. The re-establishment of overflow of Lake Victoria occurred at 14.5-14 ka BP [*Williams et al.*, 2006] while overflow at Lake Tana is dated to 15.3 ka BP [*Marshall et al.*, 2011]. The desiccation and subsequent overflow of Lakes Victoria and Tana is the main feature captured by the XRF records rather than the AHP. Likely, the XRF records are mainly sensitive to conditions at Lake Tana as the majority of Nile River sediment derives from the Ethiopian highlands [*Foucault and Stanley*, 1989].

A final hydroclimate proxy is provided by the MS record. Bulk soil MS provides a proxy for rainfall based on the premise that MS reflects the degree of pedogenesis, which increases with increasing rainfall [*Balsam et al.*, 2011]. Furthermore, it has been proposed that MS provides a quantitative rainfall proxy when appropriate statistical models are developed and calibrated for a specific region, necessary because relationships between MS and rainfall may be either linear or non-linear [*Maher and Possolo*, 2013]. We find that the GeoB7702-3 MS record is in close agreement with the δD_{wax} record, supporting its use as a rainfall proxy (Fig. 4). A modern calibration study and model of the MS-rainfall relationship has not yet been conducted for the Nile River Basin and thus we cannot calculate paleo-precipitation amounts from the MS record. However, it appears this is a promising avenue of future research. To date the MS-precipitation proxy has been studied in soils but our results suggest it also may be applicable to marine settings receiving a large influx of terrestrial material, such as the EM Sea.

4.3. Proxy responses to hydroclimate variability

An interesting feature of our data is that individual proxies analyzed on the same samples reveal differences in their responses (abrupt or gradual) to the same hydroclimate events. For example, if we had only examined brGDGTs (MAAT and soil pH), we would conclude that the AHP in the Nile Basin was a gradual event (Fig. 4). Likewise, if we had only examined δD_{wax} we might conclude that an abrupt event occurred from ca. 9-7 ka BP (Fig. 4). Thus the onset and termination of the AHP at a single site may be mutually registered as both an abrupt and gradual climate transition, depending on proxy used. Such differences among proxies are not unexpected as each has its own set of associated uncertainties and potential confounding factors, and different parts of the ecosystem (e.g. soils versus vegetation) may not exhibit the same response to environmental variability. Furthermore, different organic compound classes within the same sample can represent material of different ages as indicated by compound-specific radiocarbon investigations [*Eglinton et al.*, 1997].

A wide variety of proxies have been utilized at different locations to investigate the AHP, with some studies using a single proxy only, raising the possibility that some of the disagreement surrounding the abruptness of the AHP between studies may be partially related to the type of proxy examined. Although the Nile River integrates material along a vast, climatically diverse, catchment and thus perhaps is a non-ideal setting to examine differences in proxy response to a single event, multiproxy studies from lacustrine sites lend support this idea. At Lake Victoria, the transition to the AHP is marked by an abrupt 23‰ shift in δD_{wax} occurring in 600 years and concurrently pollen assemblages indicate an abrupt shift from a grass dominated ecosystem to a tree and shrub dominated ecosystem [*Berke et al.*, 2012]. In contrast, $\delta^{13}C_{wax}$ values remain unchanged through this transition [*Berke et al.*, 2012]. At Lake Tana, Ti XRF counts (a proxy for drought) indicate aridity during the Younger Dryas but δD_{wax} exhibits little variability at this time; additionally, the duration of humid conditions recorded by these two proxies differs [*Costa et al.*, 2014]. The Lake Challa record displays significant differences between δD_{wax}, which indicates an abrupt onset and termination of the AHP, and the BIT Index (used as a runoff proxy at this site), which exhibits a more gradual transition from the early- to mid-Holocene [*Tierney et al.*, 2011a]. These examples demonstrate that different proxies measured at a single site can record varying abrupt or gradual responses to, or different durations of, the same event. As more high-resolution paleoclimate records continue to be generated, differences in the sensitivity of individual proxies to environmental variability is a factor that should be considered with regard to the debate surrounding the abruptness of the AHP. Future multiproxy investigations, as well as compound-specific ^{14}C investigations, will help further elucidate the responses of individual proxies to hydroclimate events.

4.4. The African Humid Period

The transition from arid conditions of the Late Pleistocene into the wet phase of the early Holocene at our core site is documented by multiple hydroclimate proxies although variability in the timing and duration of the transition into and out of the AHP is evident (Figs. 4, 5). While a gradual 2° C increase in MAAT occurred from 14 to ca. 8 ka BP followed by a 2.5° C decease until 4 ka BP (Fig. 4d), most other proxies indicate a more rapid or abrupt transition at ca. 11 ka BP. The overall structure of our δD_{wax} record, which exhibits an appreciable 40‰ decrease from 11 to 9.1 ka, follows the Ba/Ca record of *Weldeab et al.* [2014] (Fig. 5), a proxy used to track Nile discharge, reflecting gradual hydroclimate change in response to orbital forcing and associated migrations of the tropical rainbelt. $\delta^{18}O$ records of the planktonic foraminifer *G. ruber* from the EM Sea, reflecting variability in Nile River discharge, indicate a similar pattern with peak runoff in the early Holocene followed by a gradual decline in runoff tracking insolation [*Hennekam et al.*, 2014; *Blanchet et al.*, 2014]. However, abrupt responses are also evident in our records. Between 9.7 and 9.1 ka BP, δD_{wax} values decrease by 20‰ in ca. 600 years. Likewise, between 7.5 and 6.7 ka BP, a 20‰ increase in δD_{wax} is noted. Thus, in the Nile Basin δD_{wax} record, the peak phase of the AHP occurred from ca. 9 to 7 ka BP and its onset and termination were abrupt. The soil pH, MS and EM SST records (Fig. 4e, 4g, 4h) also indicate an excursion during this peak phase of the AHP. In each of these records the abrupt transitions into and out of the peak humid phase are superimposed on a longer, more progressive shift in East African hydroclimate.

The external cause of the AHP is attributed to increased northern hemisphere summer insolation and associated feedbacks, which intensified land-sea temperature gradients and summer monsoonal circulation, and shifted the tropical rainbelt to the north during boreal summer [*Kutzbach and StreetPerrott*, 1985; *Claussen et al.*, 1999]. However, it is recognized that migrations of the tropical rainbelt likely were not the sole cause of hydrological fluctuations [*Tierney and deMenocal*, 2013; *Stager et al.*, 2011]. Recent studies have provided evidence for the role of the Congo Air Boundary (CAB) in modulating precipitation and contributing to abrupt hydroclimate variability in East Africa [*Tierney et al.*, 2011a; *Junginger et al.*, 2014; *Costa et al.*, 2014]. Precipitation over the Nile Basin derives from Atlantic and Indian Ocean sources [*Gimeno et al.*, 2010; *Camberlin*, 2009; *Tierney et al.*, 2011b]. At the present day, precipitation in the Congo Basin is depleted (by about -25‰) in comparison to Indian Ocean-derived precipitation falling at Lake Challa (Kenya/Tanzania) [*Tierney et al.*, 2011b]. A modeling study of Eemian African tropical and subtropical moisture transport concluded that stronger moisture advection from the Atlantic resulted in isotopically depleted rainfall in East Africa [*Herold and Lohmann*, 2009]. The Eemian scenario can be considered an analog to the early Holocene AHP. The authors found that differential surface heating occurs driven by excess NH summer insolation, which warms North Africa and increases the meridional temperature gradient [*Herold and Lohmann*, 2009]. In turn, this produces a pressure gradient and induces increased zonal flow. The enhanced zonal flow delivers a greater amount of moisture from the Atlantic to East Africa [*Herold and Lohmann*, 2009].

We suggest that the abrupt shift in the δD_{wax} record from 9-7 ka BP could result from a shift in the dominant moisture source, consistent with the model described above. A switch in the dominant moisture source is a mechanism that can account for abrupt isotopic changes thereby contributing to non-linear behavior of δD_{wax}. The Nile Basin δD_{wax} record points to increased inputs of Atlantic Ocean-derived moisture (i.e., depleted δD) during the peak phase (9-7 ka BP) of the AHP, which could result from an eastward shifted CAB. Indeed, recent studies provide evidence that during the early Holocene the CAB delivered more Atlantic derived moisture to parts of the East African Rift Valley presently located outside of the influence of the CAB [*Junginger et al.*, 2014; *Costa et al.*, 2014]. The abrupt excursion to the lowest δD_{wax} values of the entire record from ca. 7-9 ka BP may reflect a shift to relatively larger inputs of Atlantic Ocean sourced moisture within the Nile Basin, in combination with increased precipitation amount driven by increased northern hemisphere summer insolation.

4.5. Heinrich Stadial 1

Our multiproxy records reveal that a number of striking hydroclimate changes occurred in the Nile Basin during the transition from the LGM to the Holocene with the most severe aridity occurring during Heinrich Stadials (HS) (Fig. 4), in agreement with previous studies [*Stager et al.*, 2011; *Mulitza et al.*, 2008; *Tierney and deMenocal*, 2013; *Tierney et al.*, 2008]. A remarkable feature is observed during HS1 (ca. 19-14.6 ka BP [*Stanford et al.*, 2011]) as the onset and termination of this event in the δD_{wax} and MS records occurs prior to the onset of HS1 noted in the soil pH, MAAT, XRF or EM SST records (Fig. 4 & 6), suggesting two distinct phases occurring within HS1. In nearly all records HS1 is registered as abrupt event with the onset and termination occurring over ca. 200 to 1,000 years. We cannot rule out potential age discrepancies between different proxies; however, the timing of two phases observed in the Nile Basin records is in good agreement with other studies that have noted a two-phase HS1 recorded by a single proxy [*Bard et al.*, 2000]. Thus, our data lend support to a growing body of evidence that HS1 evolved in two [*Naughton et al.*, 2009; *Broecker and Putnam*, 2012] or three distinct phases [*Bouimetarhan et al.*, 2012; *Stanford et al.*, 2011; *Bard et al.*, 2000]. Hereafter we refer to the earlier phase of HS1 interval as HS1a (ca. 17.5 to 16 ka BP) and the latter phase (ca. 16-14.5 ka BP) as HS1b (Fig. 4 and 6).

High δD_{wax} values during HS1a could result from increased temperature, a shift in the dominant vegetation type, a precipitation reduction or a shift in the dominant moisture source. Temperature can be excluded as the interval prior to ca. 16 ka BP is characterized by the lowest SST and MAATs of the entire record. Similarly, vegetation is not the main factor contributing to deuterium enrichment as discussed previously. As other Nile Basin proxies and numerous North African paleoclimate records indicate maximum aridity occurring during HS1b (Fig. 4, discussion below), a precipitation reduction is unlikely to be the sole cause of the excursion to maximum δD_{wax} values. We therefore suggest that during HS1a the Nile Basin experienced a shift in the dominant moisture source and received relatively less inputs of Atlantic-derived moisture or greater amounts of Indian Ocean-derived moisture. Furthermore, although chronological differences cannot be ruled out when comparing multiple sites, we note that the excursion in the Nile Basin δD_{wax} record during HS1a appears to be synchronous with the Lake Tanganyika δD_{wax} record [*Tierney et al.,* 2008], which mainly falls under the influence of the Indian Ocean, where

HS1 terminates at 15.8 ka BP (Fig. 5c and f). A westward shifted position of the CAB could produce such an isotopic shift over the Nile Basin.

The most extreme aridity of the past 28 ka BP in North Africa occurred during HS1b, coincident with the pronounced interval of minimum SSTs in the EM [*Castañeda et al.*, 2010] and Red Seas [*Arz et al.*, 2003]. The role of EM SST in influencing rainfall in North Africa, on decadal or longer timescales, is well-established [*Rowell*, 2003]. Low EM SST reduces the moisture content of the lower troposphere, leading to reduced southward moisture advection and decreased low-level moisture convergence over the Sahel, thereby reducing precipitation [*Rowell*, 2003]. Synchronous with low EM SST, a major excursion is seen in the XRF elemental ratios (Fig. 4), attributed to the desiccation of Lakes Tana [*Marshall et al.*, 2011] and Victoria [*Stager et al.*, 2011] and a dramatic reduction in Nile flow. During Heinrich Stadials, reduced Atlantic Meridional Overturning Circulation (AMOC) and associated North Atlantic cooling caused a southward shift of the tropical rainbelt, stronger NE trade winds, and intensified moisture export by the African Easterly Jet [*Mulitza et al.*, 2008]. The NE trade winds were particularly strong during the latter part of HS1, from ca. 16-15 ka BP, as was the African Easterly Jet (AEJ), increasing moisture export from continental Africa [*Bouimetarhan et al.*, 2012; *Mulitza et al.*, 2008] (Fig. 6). In the Arabian Peninsula region exceptionally dry and dusty conditions are noted during HS1b [*Deplazes et al.*, 2014].

Interestingly, the Nile Basin MBT'/CBT MAAT record indicates increased temperatures during the HS1b interval, coincident with low SST observed in the EM [*Castañeda et al.*, 2010] and Red Seas [*Arz et al.*, 2003]. It is unlikely that the Nile Basin experienced warming at this time. Rather, the apparent warming is attributed to an equatorward shift in the dominant source area of material transported by the Nile River following the desiccation of Lake Tana with decreased runoff from the colder Ethiopian Highlands and relatively higher contributions of White Nile material (Figs. 3, 4).

4.6. Influence of hydroclimate variability on human populations

The dramatic hydroclimate changes that took place in North Africa during the AHP had a major impact on human populations as documented by the archaeological record [*Kuper and Kröpelin*, 2006; *Vermeersch and Van Neer*, 2015]. We note that the peak phase of the AHP in the Nile Basin corresponds to the abandonment of settlements in the Nile Valley of Egypt (Fig. 5), likely due to the prevalence of hazardous flood events along the Nile [*Kuper and Kröpelin*, 2006]. The termination of the peak AHP phase is consistent with the reoccupation of Nile Valley settlements at 7.5 ka BP. In the late Holocene, the Old World Kingdom collapsed at ca. 4.2 ka BP [*Stanley et al.*, 2003]. High variability is observed in some of the Nile Basin records during the late Holocene, particularly in the soil pH and δD_{wax} records, likely reflecting alternating floods and droughts that are registered in Egyptian chronology [*Stanley et al.*, 2003].

Two main periods of human occupation are recognized in the Upper Egyptian Nile Valley during the Late Pleistocene; around the LGM (23-20 ka BP) and around HS1 (ca. 16-14 ka BP) [*Vermeersch and Van Neer*, 2015]. At these times, it is hypothesized that aeolian sands created dams at several places along the Nile, allowing for the formation of lakes and suitable environments for human occupation in an otherwise extremely arid setting [*Vermeersch and Van Neer*, 2015]. The influence of aridity during HS1 on human populations is debated [*Stager et al.*, 2011; *Thomas et al.*, 2012]. *Stager et al.* [2011]

describe HS1 as "one of the most intense and extensive" droughts of the past 50 ka and hypothesize that this event had a major impact on Paleolithic cultures. Conversely, *Thomas et al.* [2012] note that across the African continent conditions are variable at the time of HS1 and instead postulate that environmental variability played a major role in influencing modern human behavior and evolution. While our new records cannot directly address this debate, certainly a large portion of East Africa north of the equator experienced abrupt and severe aridity during HS1 including the Nile Basin.

5. Conclusions

Our multi-proxy study demonstrates that dramatic hydroclimate variability occurred in Nile Basin during the past 28,000 years. Overall, our new Nile Basin records support other North African hydroclimate records while providing information regarding shifts in the dominant sources of material delivered to the EM Sea via the Blue Nile and the White Nile. While δD_{wax} is often interpreted to reflect precipitation amount in the African tropics, our data suggest that shifting moisture sources, related to migrations of the tropical rainbelt and CAB, also contributed to isotopic variability. As δD_{wax} may behave non-linearly due to the additional influence of changing moisture sources, care should be taken when interpreting δD_{wax} records from areas falling under the influence of isotopically distinct moisture sources. We note that at several North African sites, hydroclimate records reveal both abrupt and gradual responses to single events and these differential responses appear to be proxy-dependent, potentially contributing to the debate surrounding the abruptness of the AHP. Our new records provide strong evidence for severe aridity in the Nile Basin during HS1, an event that evolved in two phases, whereas maximum wet conditions occurred during the AHP from ca. 9-7 ka BP. Zonal migrations of the CAB likely contributed to the extreme hydroclimate fluctuations observed during these events, which may have impacted Paleolithic cultures residing along the Nile corridor.

Acknowledgements

We thank Marianne Baas, Ellen Hopmans, Jort Ossebaar and Michiel Kienhuis for analytical assistance. We thank two anonymous reviewers for thoughtful comments that improved the manuscript. Research funding was provided by NEBROC-2. Samples from GeoB7702-3 were supplied through the assistance of the University of Bremen, Geosciences Department and MARUM. This work was supported by the DFG-Research Center/Excellence Cluster "The Ocean in the Earth System".

References

Amit, R., Y. Enzel, O. Crouvi, O. Simhai, A. Matmon, N. Porat, E. McDonald, and A. R. Gillespie (2011), The role of the Nile in initiating a massive dust influx to the Negev late in the middle Pleistocene, *Geological Society of America Bulletin*, *123*(5-6), 873–889.

Arz, H. W., J. Pätzold, P. J. Müller, and M. O. Moammar (2003), Influence of Northern Hemisphere climate and global sea level rise on the restricted Red Sea marine environment during termination I, *Paleoceanography*, *18*(2).

Balsam, W. L., B. B. Ellwood, J. Ji, E. R. Williams, X. Long, and A. El Hassani (2011), Magnetic susceptibility as a proxy for rainfall: worldwide data from tropical and temperate climate, *Quaternary Science Reviews*, *30*(19), 2732–2744.

Bard, E. (2013), Out of the African Humid Period, *Science*, *342*(6160), 808–809.

Bard, E., F. Rostek, J.-L. Turon, and S. Gendreau (2000), Hydrological impact of Heinrich events in the subtropical northeast Atlantic, *Science*, *289*(5483), 1321–1324.

Ben Israel, M., Y. Enzel, and Y. Erel (2015), Provenance of the various grain-size fractions in the Negev loess and potential changes in major dust sources to the Eastern Mediterranean, *Quaternary Research*, *83*(1), 105–115.

Berke, M. A., T. C. Johnson, J. P. Werne, K. Grice, S. Schouten, and J. S. Sinninghe Damsté (2012), Molecular records of climate variability and vegetation response since the Late Pleistocene in the Lake Victoria basin, East Africa, *Quaternary Science Reviews*, *55*, 59–74.

Blanchet, C. L., R. Tjallingii, M. Frank, J. Lorenzen, A. Reitz, K. Brown, T. Feseker, and W. Brückmann (2013), High-and low-latitude forcing of the Nile River regime during the Holocene inferred from laminated sediments of the Nile deep-sea fan, *Earth and Planetary Science Letters*, *364*, 98–110.

Blanchet, C. L., M. Frank, and S. Schouten (2014), Asynchronous changes in vegetation, runoff and erosion in the Nile River Watershed during the Holocene, *PLoS ONE*, *9*(12), e115,958, doi:10.1371/journal.pone. 0115958.

Bouimetarhan, I., M. Prange, E. Schefuß, L. Dupont, J. Lippold, S. Mulitza, and K. Zonneveld (2012), Sahel megadrought during Heinrich Stadial 1: evidence for a three-phase evolution of the low-and midlevel West African wind system, *Quaternary Science Reviews*, *58*, 66–76.

Box, M., M. Krom, R. Cliff, M. Bar-Matthews, A. Almogi-Labin, A. Ayalon, and M. Paterne (2011), Response of the Nile and its catchment to millennial-scale climatic change since the LGM from Sr isotopes and major elements of East Mediterranean sediments, *Quaternary Science Reviews*, *30*(3), 431–442.

Broecker, W., and A. E. Putnam (2012), How did the hydrologic cycle respond to the two-phase mystery interval?, *Quaternary Science Reviews*, *57*, 17–25.

Camberlin, P. (2009), Nile Basin Climates, in *The Nile*, pp. 307–333, Springer.

Castañeda, I. S., S. Mulitza, E. Schefuß, R. A. L. dos Santos, J. S. Sinninghe Damsté, and S. Schouten (2009), Wet phases in the Sahara/Sahel region and human migration patterns in North Africa, *Proceedings of the National Academy of Sciences*, *106*(48), 20,159–20,163.

Castañeda, I. S., E. Schefuß, J. Pätzold, J. S. Sinninghe Damsté, S. Weldeab, and S. Schouten (2010), Millennial-scale sea surface temperature changes in the eastern Mediterranean (Nile River Delta region) over the last 27,000 years, *Paleoceanography*, *25*(1).

Claussen, M., C. Kubatzki, V. Brovkin, A. Ganopolski, P. Hoelzmann, and H.-J. Pachur (1999), Simulation of an abrupt change in Saharan vegetation in the mid-Holocene, *Geophysical Research Letters*, *26*(14), 2037–2040.

Costa, K., J. Russell, B. Konecky, and H. Lamb (2014), Isotopic reconstruction of the African Humid Period and Congo Air Boundary migration at Lake Tana, Ethiopia, *Quaternary Science Reviews*, *83*(0), 58 – 67, doi:http://dx.doi.org/10.1016/j.quascirev.2013.10.031.

Dansgaard, W. (1964), Stable isotopes in precipitation, *Tellus*, *16*(4), 436– 468.

deMenocal, P., J. Ortiz, T. Guilderson, J. Adkins, M. Sarnthein, L. Baker, and M. Yarusinsky (2000), Abrupt onset and termination of the African Humid Period:: rapid climate responses to gradual insolation forcing, *Quaternary Science Reviews*, *19*(15), 347 – 361, doi:http://dx.doi.org/ 10.1016/S0277-3791(99)00081-5.

Deniel, C., and C. Pin (2001), Single–stage method for the simultaneous isolation of lead and strontium from silicate samples for isotopic measurements, *Analytica Chimica Acta*, *426*(1), 95–103.

Deplazes, G., A. Lückge, J.-B. W. Stuut, J. Pätzold, H. Kuhlmann, D. Husson, M. Fant, and G. H. Haug (2014), Weakening and strengthening of the Indian monsoon during Heinrich events and Dansgaard-Oeschger oscillations, *Paleoceanography*, *29*(2), 99–114.

Eglinton, G., and R. J. Hamilton (1967), Leaf epicuticular waxes, *Science*, *156*(3780), 1322–1335.

Eglinton, T. I., Benitez-Nelson, B. C., Pearson, A., McNichol, A. P., Bauer, J. E., and Druffel, E. R. (1997), Variability in radiocarbon ages of individual organic compounds from marine sediments. *Science, 277*, 796-799.

Foucault, A., and D. J. Stanley (1989), Late Quaternary palaeoclimatic oscillations in East Africa recorded by heavy minerals in the Nile delta, *Nature*, *339*, 44–46.

Gimeno, L., A. Drumond, R. Nieto, R. M. Trigo, and A. Stohl (2010), On the origin of continental precipitation, *Geophysical Research Letters*, *37*(13).

Hennekam, R., T. Jilbert, B. Schnetger, and G. J. Lange (2014), Solar forcing of Nile discharge and sapropel S1 formation in the early to middle Holocene eastern Mediterranean, *Paleoceanography*, *29*(5), 343–356.

Herold, M., and G. Lohmann (2009), Eemian tropical and subtropical African moisture transport: an isotope modelling study, *Climate dynamics*, *33*(7-8), 1075–1088.

Junginger, A., S. Roller, L. A. Olaka, and M. H. Trauth (2014), The effects of solar irradiation changes on the migration of the Congo Air Boundary and water levels of paleo-Lake Suguta, Northern Kenya Rift, during the African Humid Period (15–5 ka BP), *Palaeogeography, Palaeoclimatology, Palaeoecology*, *396*(0), 1 – 16, doi:http://dx.doi.org/10.1016/j. palaeo.2013.12.007.

Kim, J.-H., S. Schouten, M. Rodrigo-Gámiz, S. Rampen, G. Marino, C. Huguet, P. Helmke, R. Buscail, E. C. Hopmans, J. Pross, F. Sangiorgi, J. B. Middelburg, and J. S. Sinninghe Damsté (2015), Influence of deepwater derived isoprenoid tetraether lipids on the paleothermometer in the Mediterranean Sea, *Geochimica et Cosmochimica Acta*, *150*(0), 125 – 141, doi:http://dx.doi.org/10.1016/j.gca.2014.11.017.

Krom, M. D., J. D. Stanley, R. A. Cliff, and J. C. Woodward (2002), Nile River sediment fluctuations over the past 7000 yr and their key role in sapropel development, *Geology*, *30*(1), 71–74.

Kuhlmann, H., H. Meggers, T. Freudenthal, and G. Wefer (2004), The transition of the monsoonal and the N Atlantic climate system off NW Africa during the Holocene, *Geophysical Research Letters*, *31*(22), L22,204.

Kuper, R., and S. Kröpelin (2006), Climate-controlled Holocene occupation in the Sahara: motor of Africa's evolution, *Science*, *313*(5788), 803–807.

Kutzbach, J. E., and F. A. Street-Perrott (1985), Milankovitch forcing of fluctuations in the level of tropical lakes from 18 to 0 kyr BP, *Nature*, *317*, 130–134.

Lamb, H. F., C. R. Bates, P. V. Coombes, M. H. Marshall, M. Umer, S. J. Davies, and E. Dejen (2007), Late Pleistocene desiccation of Lake Tana, source of the Blue Nile, *Quaternary Science Reviews*, *26*(3), 287–299.

Laskar, J., P. Robutel, F. Joutel, M. Gastineau, A. Correia, B. Levrard, et al. (2004), A long-term numerical solution for the insolation quantities of the Earth, *Astronomy & Astrophysics*, *428*(1), 261–285.

Maher, B., and A. Possolo (2013), Statistical models for use of palaeosol magnetic properties as proxies of palaeorainfall, *Global and Planetary Change*, *111*, 280–287.

Marshall, M. H., H. F. Lamb, D. Huws, S. J. Davies, R. Bates, J. Bloemendal, J. Boyle, M. J. Leng, M. Umer, and C. Bryant (2011), Late Pleistocene and Holocene drought events at Lake Tana, the source of the Blue Nile, *Global and Planetary Change*, *78*(3), 147–161.

McGee, D., P. deMenocal, G. Winckler, J. Stuut, and L. Bradtmiller (2013), The magnitude, timing and abruptness of changes in North African dust deposition over the last 20,000 yr, *Earth and Planetary Science Letters*, *371*, 163–176.

Mikova, J., and P. Denkova (2007), Modified chromatographic separation scheme for Sr and Nd isotope analysis in geological silicate samples, *Journal of Geosciences*, *52*(3-4), 221–226.

Muhs, D. R., J. Roskin, H. Tsoar, G. Skipp, J. R. Budahn, A. Sneh, N. Porat, J.-D. Stanley, I. Katra, and D. G. Blumberg (2013), Origin of the Sinai–Negev erg, Egypt and Israel: mineralogical and geochemical evidence for the importance of the Nile and sea level history, *Quaternary Science Reviews*, *69*, 28–48.

Mulitza, S., M. Prange, J.-B. Stuut, M. Zabel, T. von Dobeneck, A. C. Itambi, J. Nizou, M. Schulz, and G. Wefer (2008), Sahel megadroughts triggered by glacial slowdowns of Atlantic meridional overturning, *Paleoceanography*, *23*(4).

Naughton, F., M. Sánchez Goñi, M. Kageyama, E. Bard, J. Duprat, E. Cortijo, S. Desprat, B. Malaizé, C. Joly, F. Rostek, et al. (2009), Wet to dry climatic trend in north-western Iberia within Heinrich events, *Earth and Planetary Science Letters*, *284*(3), 329–342.

Pätzold, J., G. Bohrmann, and C. Hübscher (2003), Black Sea - Mediterranean - Red Sea, Cruise No. 52, January 2 - March 27, 2002, Istanbul - Limassol. METEOR–Berichte 03-2, *Universität Hamburg*, p. 178 pp.

Peterse, F., J. van der Meer, S. Schouten, J. W. Weijers, N. Fierer, R. B. Jackson, J.-H. Kim, and J. S. Sinninghe Damsté (2012), Revised calibration of the MBT–CBT paleotemperature proxy based on branched tetraether membrane lipids in surface soils, *Geochimica et Cosmochimica Acta*, *96*, 215–229.

Pin, C., D. Briot, C. Bassin, and F. Poitrasson (1994), Concomitant separation of strontium and samarium-neodymium for isotopic analysis in silicate samples, based on specific extraction chromatography, *Analytica Chimica Acta*, *298*(2), 209–217.

Revel, M., E. Ducassou, F. Grousset, S. Bernasconi, S. Migeon, S. Revillon, J. Mascle, A. Murat, S. Zaragosi, and D. Bosch (2010), 100,000 years of African monsoon variability recorded in sediments of the Nile margin, *Quaternary Science Reviews*, *29*(11), 1342–1362.

Risi, C., S. Bony, and F. Vimeux (2008), Influence of convective processes on the isotopic composition (δ^{18}O and δD) of precipitation and water vapor in the tropics: 2. physical interpretation of the amount effect, *Journal of Geophysical Research: Atmospheres*, *113*(D19), 1984–2012.

Rowell, D. P. (2003), The impact of Mediterranean SSTs on the Sahelian rainfall season, *Journal of Climate*, *16*(5), 849–862.

Sachse, D., I. Billault, G. J. Bowen, Y. Chikaraishi, T. E. Dawson, S. J. Feakins, K. H. Freeman, C. R. Magill, F. A. McInerney, M. T. Van der Meer, et al. (2012), Molecular paleohydrology: interpreting the hydrogen-isotopic composition of lipid biomarkers from photosynthesizing organisms, *Annu. Rev. Earth Planet. Sci*, *40*, 221–249.

Schefuß, E., S. Schouten, J. F. Jansen, and J. S. Sinninghe Damsté (2003), African vegetation controlled by tropical sea surface temperatures in the mid-Pleistocene period, *Nature*, *422*(6930), 418–421.

Schefuß, E., S. Schouten, and R. R. Schneider (2005), Climatic controls on central African hydrology during the past 20,000 years, *Nature*, *437*(7061), 1003–1006.

Schefuß, E., H. Kuhlmann, G. Mollenhauer, M. Prange, and J. Pätzold (2011), Forcing of wet phases in southeast Africa over the past 17,000 years, *Nature*, *480*(7378), 509–512.

Shanahan, T. M., N. P. McKay, K. A. Hughen, J. T. Overpeck, B. OttoBliesner, C. W. Heil, J. King, C. A. Scholz, and J. Peck (2015), The time-transgressive termination of the African Humid Period, *Nature Geoscience*, *8*, 140–144.

Stager, J. C., D. B. Ryves, B. M. Chase, and F. S. Pausata (2011), Catastrophic drought in the Afro-Asian monsoon region during Heinrich event 1, *Science*, *331*(6022), 1299–1302.

Stanford, J., E. Rohling, S. Bacon, A. Roberts, F. Grousset, and M. Bolshaw (2011), A new concept for the paleoceanographic evolution of Heinrich event 1 in the North Atlantic, *Quaternary Science Reviews*, *30*(9), 1047–1066.

Stanley, J.-D., M. D. Krom, R. A. Cliff, and J. C. Woodward (2003), Short contribution: Nile flow failure at the end of the Old Kingdom, Egypt: strontium isotopic and petrologic evidence, *Geoarchaeology*, *18*(3), 395– 402.

Thomas, D. S., S. L. Burrough, and A. G. Parker (2012), Extreme events as drivers of early human behaviour in Africa? The case for variability, not catastrophic drought, *Journal of Quaternary Science*, *27*(1), 7–12.

Tierney, J. E., and M. P. Tingley (2014), A Bayesian, spatially-varying calibration model for the TEX_{86} proxy, *Geochimica et Cosmochimica Acta*, *127*, 83–106.

Tierney, J. E., J. M. Russell, Y. Huang, J. S. Sinninghe Damsté, E. C. Hopmans, and A. S. Cohen (2008), Northern hemisphere controls on tropical southeast African climate during the past 60,000 years, *Science*, *322*(5899), 252–255.

Tierney, J. E., J. M. Russell, J. S. Sinninghe Damsté, Y. Huang, and D. Verschuren (2011a), Late Quaternary behavior of the East African monsoon and the importance of the Congo Air Boundary, *Quaternary Science Reviews*, *30*(78), 798 – 807, doi:http://dx.doi.org/10.1016/j.quascirev.2011.01.017.

Tierney, J. E., S. C. Lewis, B. I. Cook, A. N. LeGrande, and G. A. Schmidt (2011b), Model, proxy and isotopic perspectives on the East African Humid Period, *Earth and Planetary Science Letters*, *307*(12), 103 –112, doi:http://dx.doi.org/10.1016/j.epsl.2011.04.038.

Tierney, J. E., and P.B. de Menocal (2013), Abrupt shifts in Horn of Africa hydroclimate since the Last Glacial Maximum, *Science*, *342*(6160), 843–846.

Vermersch, P.M., and Van Neer, W. (2015), Nile behaviour and Late Palaeolithic humans in Upper Egypt during the Late Pleistocene. *Quaternary Science Reviews (in press)*.

Wang, Y. V., G. Leduc, M. Regenberg, N. Andersen, T. Larsen, T. Blanz, and R. R. Schneider (2013), Northern and southern hemisphere controls on seasonal sea surface temperatures in the Indian Ocean during the last deglaciation, *Paleoceanography*, *28*(4), 619–632.

Weijers, J. W. H., S. Schouten, J. C. van den Donker, E. C. Hopmans, and J. S. Sinninghe Damsté (2007), Environmental controls on bacterial tetraether membrane lipid distribution in soils, *Geochim. Cosmochim. Acta*, *71*(3), 703–713, doi:10.1016/j.gca.2006.10.003.

Weldeab, S., K.-C. Emeis, C. Hemleben, and W. Siebel (2002), Provenance of lithogenic surface sediments and pathways of riverine suspended matter in the Eastern Mediterranean Sea: evidence from ($^{143}Nd/^{144}Nd$ and $^{87}Sr/^{86}Sr$ ratios, *Chemical Geology*, *186*(1), 139–149.

Weldeab, S., V. Menke, and G. Schmiedl (2014), The pace of East African monsoon evolution during the Holocene, *Geophysical Research Letters*, *41*(5), 1724–1732.

Williams, M., M. Talbot, P. Aharon, Y. Abdl Salaam, F. Williams, and K. Inge Brendeland (2006), Abrupt return of the summer monsoon 15,000 years ago: new supporting evidence from the lower White Nile valley and Lake Albert, *Quaternary Science Reviews*, *25*(19), 2651–2665.

Figure Captions

Figure 1: a) The termination of the early Holocene Humid Period in North Africa. The colored circles indicate sites where the transition out of the African Humid Period is observed to be abrupt (orange), gradual (green) or stepwise (yellow). Note that the study locations depicted by the dots are approximate and in some cases have been shifted slightly where dots overlapped. See the Supplementary Material for the full list of sites and references. b and c) Mean surface winds over Africa in January and July/August. The locations of the Intertropical Convergence Zone (ITCZ) and Congo Air Boundary (CAB) are illustrated. In b and c, the Nile River catchment is indicated by the area outlined in green and the orange star indicates the location of sediment core GeoB7702-3.

Figure 2: a) Location of core GeoB7702-3 in the Eastern Mediterranean Sea. The blue box denotes the area expanded in b) and the green shaded area indicates the catchment of the Nile River. b) Close up of the location of core GeoB7702-3. The approximate locations of cores P362/2-33 [*Blanchet et al.*, 2014], core 9509 [*Box et al.*, 2011] and SL 112 [*Weldeab et al.*, 2014] are also shown. The approximate locations of the Sinai/Negev dunes and loess is indicated by the yellow and brown shading, respectively. c) Precipitation regimes within the Nile River catchment, indicated by colors and numbers. The figure is modified from [*Camberlin*, 2009]. The location of the Blue Nile (BN), the White Nile (WN), Lake Tana (LT), and Lake Victoria (LV) are indicated. From north to south, zone 1 in the northernmost part of Egypt receives winter rains from the Mediterranean; highest rainfall in January amounts to 11 mm per month. Hereafter, the precipitation numbers provided represent the maximum monthly precipitation for each particular zone and the data derives from [*Camberlin*, 2009]. Zone 2 receives almost no precipitation throughout the year while zone 3 captures the northernmost part of the summer rainfall peak in August (27 mm). Zones 4 and 5 also experience maximum rainfall in August with zone 5 receiving more precipitation (169 mm) than zone 4 (92 mm). Continuing to the south, zone 6 in southern Sudan experiences a longer rainy season with maximum precipitation noted in August (183 mm). Zone 7 western Ethiopia is similar to zone 6 but sees maximum precipitation in July (301 mm) and August. Equatorial zones 8 and 9 experience two yearly passages of the ITCZ

and hence two rainy seasons in April (206 mm for zone 9) and November. For information regarding total annual precipitation within the Nile catchment the reader is referred to Camberlin [2009].

Figure 3: Radiogenic isotopes and sources of material to GeoB7702-3. a) The figure is based on *Blanchet et al.* [2013] and modified to include the data of *Ben Israel et al.* [2015]. Shaded areas reveal the isotopic values of material derived from the Blue and Atbara Nile, the Sobat, Negev loess, the White Nile, Erythrean and Nubian dust, Saharan and Lybian dust and the Victoria and Albert Nile. All samples of GeoB7702-3 are clearly distinguished from those of dust sources and plot between Blue and White Nile endmembers. b) GeoB7702-3 neodymium (light green squares) and strontium (teal triangles) isotopes. Note the close agreement of the GeoB7702-3 strontium isotope record with that from core 9509 (light blue squares; see Fig. 2 for the location of this core), also collected from the Eastern Mediterranean Sea [*Box et al.*, 2011].

Figure 4: Selected geochemical records from GeoB7702-3. The gray shading highlights Heinrich Stadials (HS) 1 and 2 and the African Humid Period. Two intervals within HS1, HS1a and HS1b, are indicated by the shading. a) Element intensity ratio of iron (Fe) to aluminum (Al). b) Element intensity ratio of titanium (Ti) to calcium (Ca). c) Leaf wax carbon isotopes ($\delta^{13}C_{wax}$) measured on the C_{31} *n*-alkane, the dominant homologue present. d) Mean annual air temperature reconstructed using the MBT'/CBT proxy. e) TEX_{86} temperature reconstruction from *Castañeda et al.* [2010] plotted using the calibration of *Tierney and Tingley* [2014]. e) $^{87}Sr/^{86}Sr$ isotope ratio. The arrow indicates relative contributions from the White and Blue Nile. f) Leaf wax deuterium isotopes (δD_{wax}) measured on the C_{31} *n*-alkane corrected for ice volume changes. Lower values are interpreted as indicated increased rainfall or increased input of Atlantic-derived moisture. g) Volume specific magnetic susceptibility (MS) in e^{-5} SI units. It has been suggested that MS provides a rainfall proxy with higher MS values associated with higher rainfall [*Balsam et al.*, 2011]. h) Soil pH reconstructed from the CBT index. Lower (more acidic) values are indicative of wetter conditions. i) Summer (June, July and August) insolation at 15°N [*Laskar et al.*, 2004].

Figure 5: The African Humid Period (AHP). a) June, July and August (JJA) insolation at 15°N [*Laskar et al.*, 2004]. b) Ba/Ca record of *G. ruber* in the Levantine Basin of the Eastern Mediterranean Sea from *Weldeab et al.* [2014]. c) Nile Basin δD_{wax}. Note the abrupt excursion to lower values during the peak phase of the AHP, indicated by the arrow and gray shading. d) Congo Basin δD_{wax} [*Schefuß et al.*, 2005]. e) Gulf of Aden δD_{wax} [*Tierney and deMenocal*, 2013]. f) Lake Tanganyika δD_{wax} [*Tierney et al.*, 2008]. g) Lake Victoria δD_{wax} [*Berke et al.*, 2012]. δD from the Nile and Congo River Basins was measured on the C_{31} *n*-alkane while the Gulf of Aden, Lake Tanganyika and Lake Victoria δD records were measured on the C_{28} fatty acid. The colored bars at the top indicate phases of occupation (O) and abandonment (A) of Nile Valley (Egypt) settlements [*Kuper and Kröpelin*, 2006; *Stanley et al.*, 2003; *Weldeab et al.*, 2014].

Figure 6: Selected records of Heinrich Stadials (HS) 1 and 2. a) The reflectance (L*) record of Arabian Sea core SO130-289KL [*Deplazes et al.*, 2014]. b) TEX_{86} SST estimates for GeoB7702-3 [*Castañeda et al.*, 2010]. c) Ice volume corrected δD_{wax} values from GeoB7702-3. d) Iron (Fe) to potassium (K) ratios from core GeoB 9508-5 near the Senegal River in West Africa [*Mulitza et al.*, 2008]. The gray shading highlights HS 1 and 2. The solid and dashed lines indicate the initiation and termination of HS1 in the GeoB7702-3 SST and δD_{wax} records, respectively. Note the ca. 1,300 year offset between HS1 as recorded in the δD_{wax} and SST records.

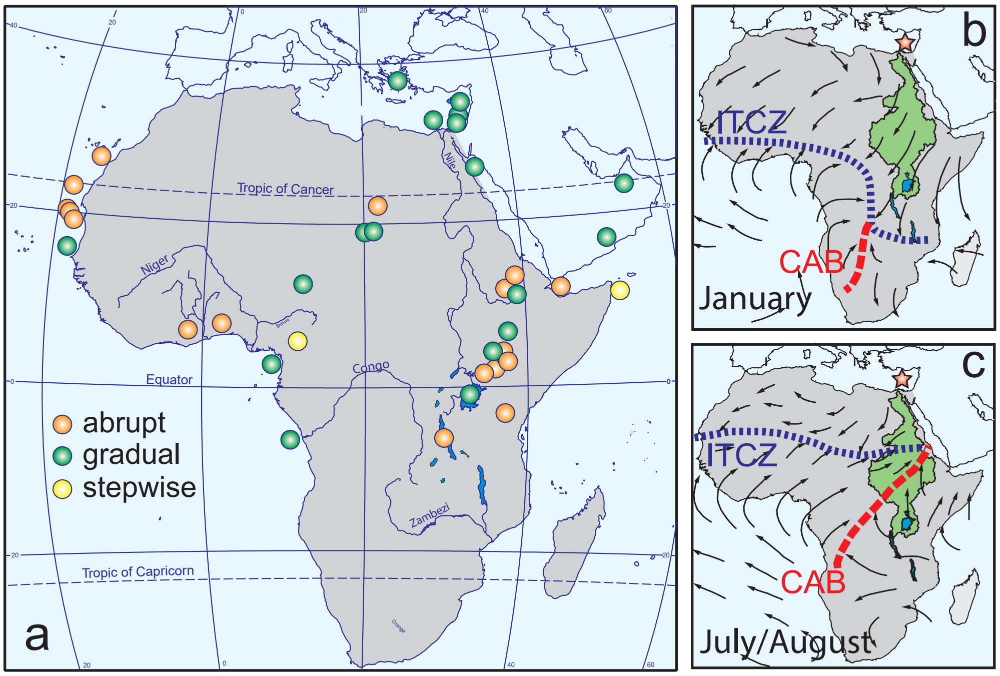
Tropic of Cancer
Niger
Nile
Equator
Congo
Zambezi
Tropic of Capricorn
abrupt
gradual
stepwise
a
b
ITCZ
CAB
January
c
ITCZ
CAB
July/August

Figure 1

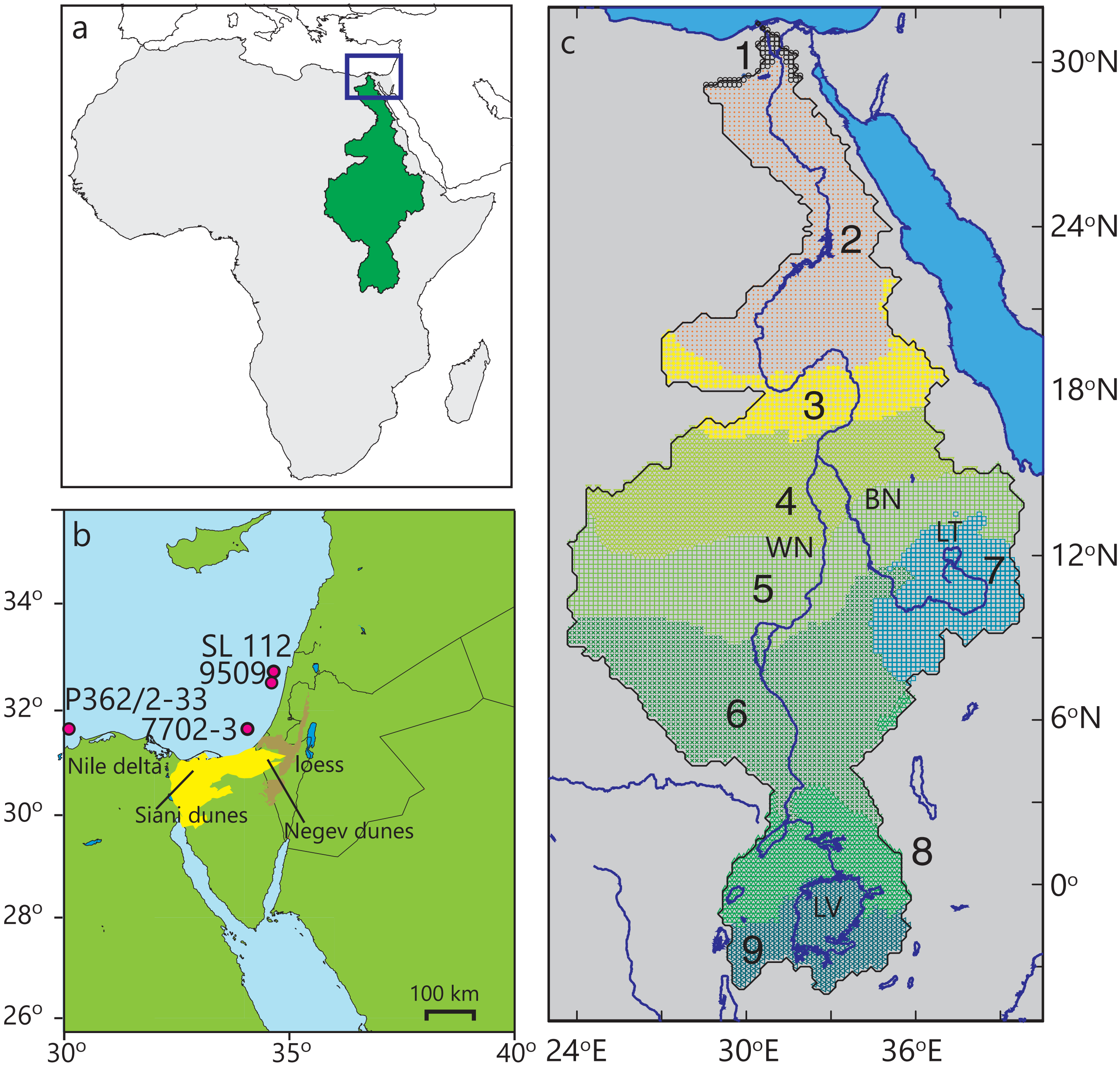
a
b
SL 112
9509
P362/2-33
7702-3
Nile delta
Siani dunes
loess
Negev dunes
100 km
34°
32°
30°
28°
26°
30°
35°
40°
c
1
2
3
4
5
6
7
8
9
BN
WN
LT
LV
30°N
24°N
18°N
12°N
6°N
0°
24°E
30°E
36°E

Figure 2

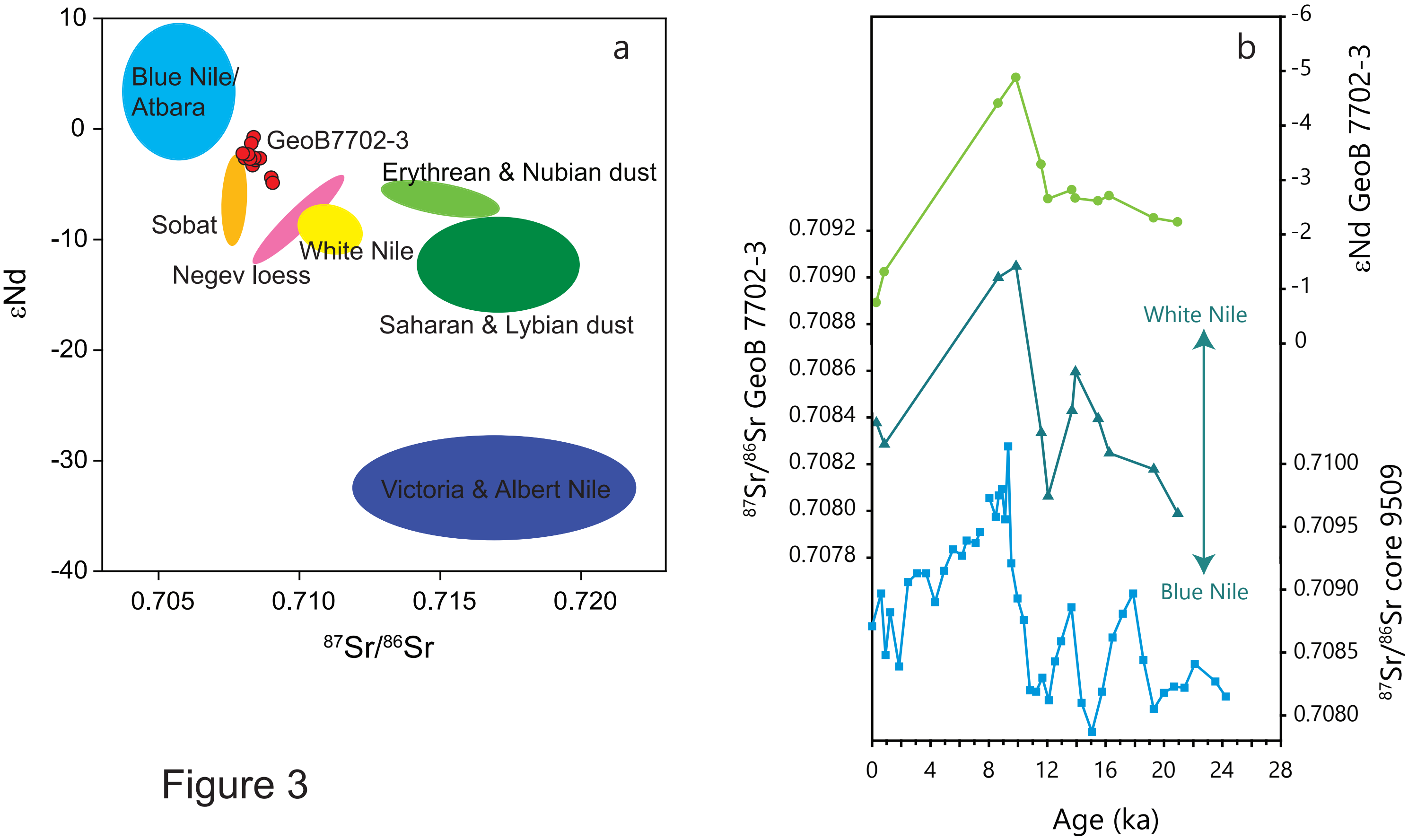

a
Blue Nile/
Atbara
GeoB7702-3
Erythrean & Nubian dust
Sobat
White Nile
Negev loess
Saharan & Lybian dust
Victoria & Albert Nile
εNd
87Sr/86Sr
b
εNd GeoB 7702-3
87Sr/86Sr GeoB 7702-3
87Sr/86Sr core 9509
White Nile
Blue Nile
Age (ka)

Figure 3

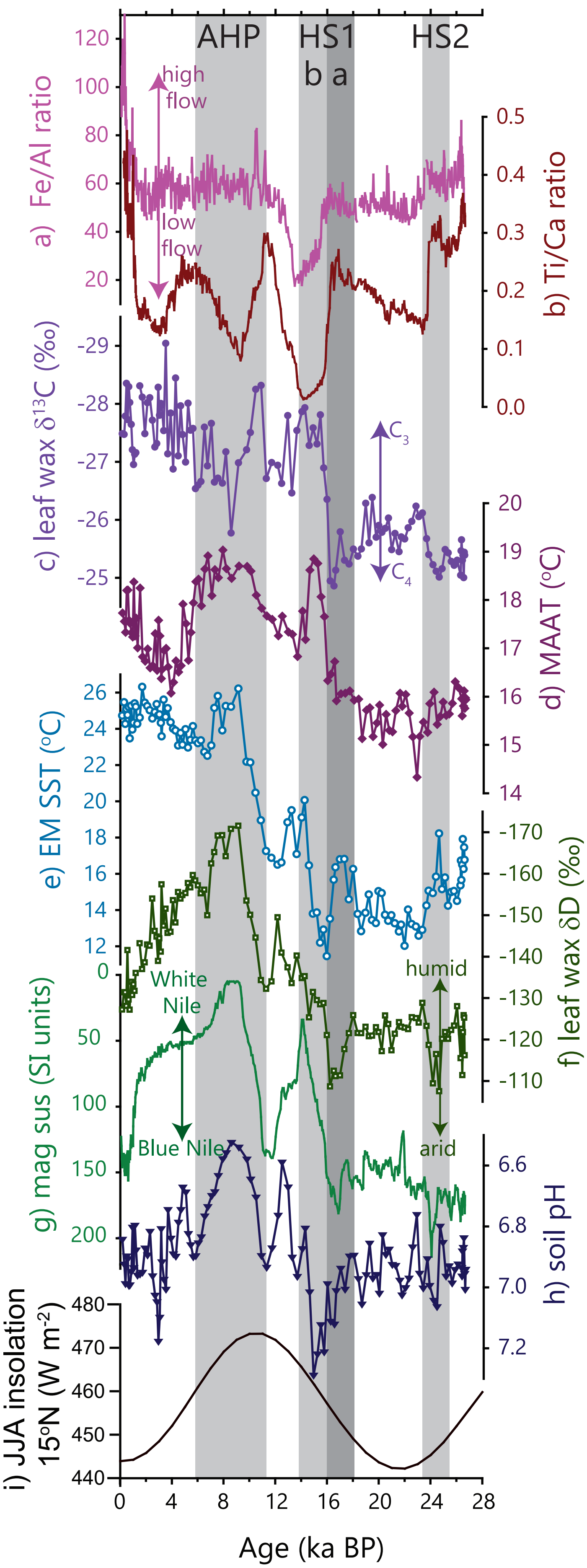

AHP
HS1
b a
HS2
a) Fe/Al ratio
high flow
low flow
b) Ti/Ca ratio
c) leaf wax δ13C (‰)
C3
C4
d) MAAT (°C)
e) EM SST (°C)
f) leaf wax δD (‰)
humid
arid
g) mag sus (SI units)
White Nile
Blue Nile
h) soil pH
i) JJA insolation 15°N (W m-2)
Age (ka BP)

Figure 4

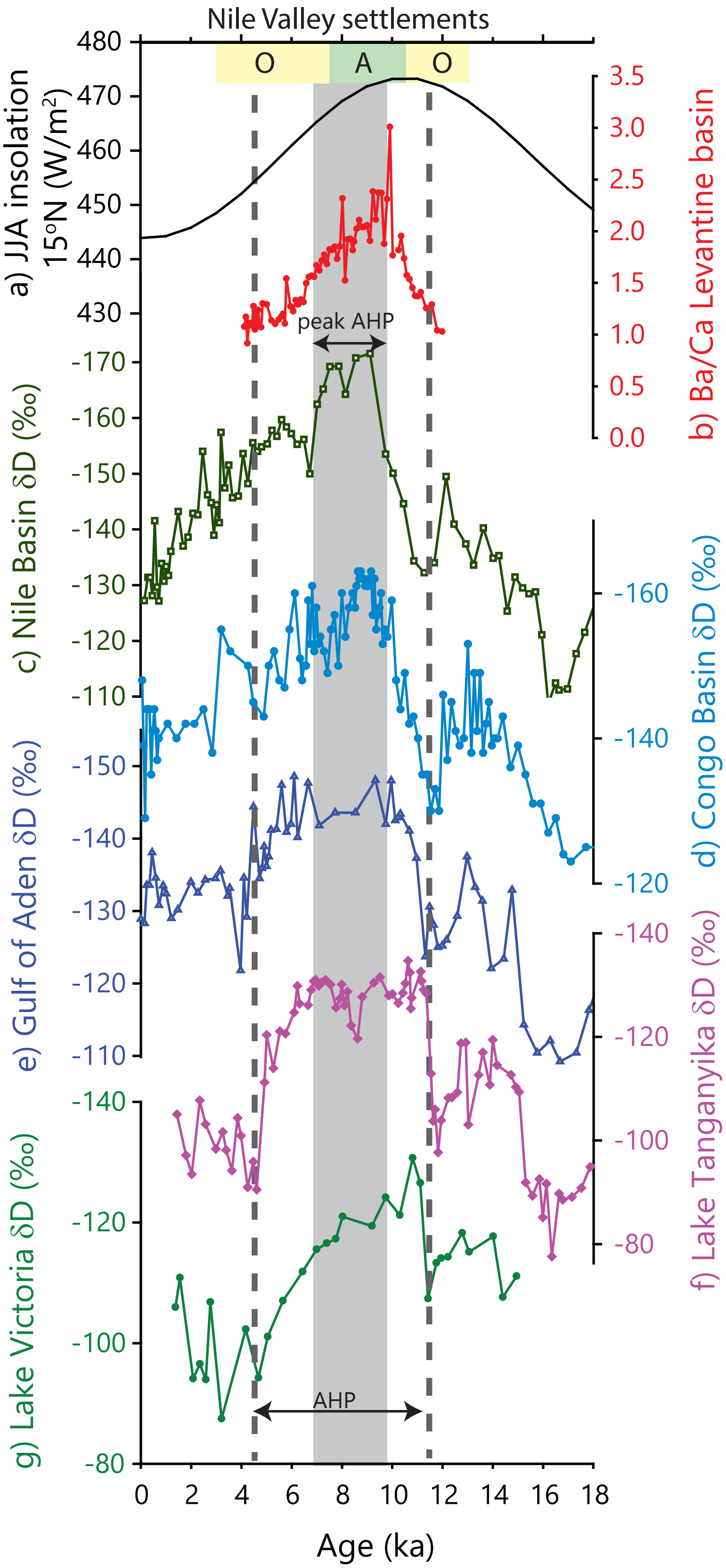

Nile Valley settlements
O
A
O
a) JJA insolation 15°N (W/m²)
b) Ba/Ca Levantine basin
peak AHP
c) Nile Basin δD (‰)
d) Congo Basin δD (‰)
e) Gulf of Aden δD (‰)
f) Lake Tanganyika δD (‰)
g) Lake Victoria δD (‰)
AHP
Age (ka)

Figure 5

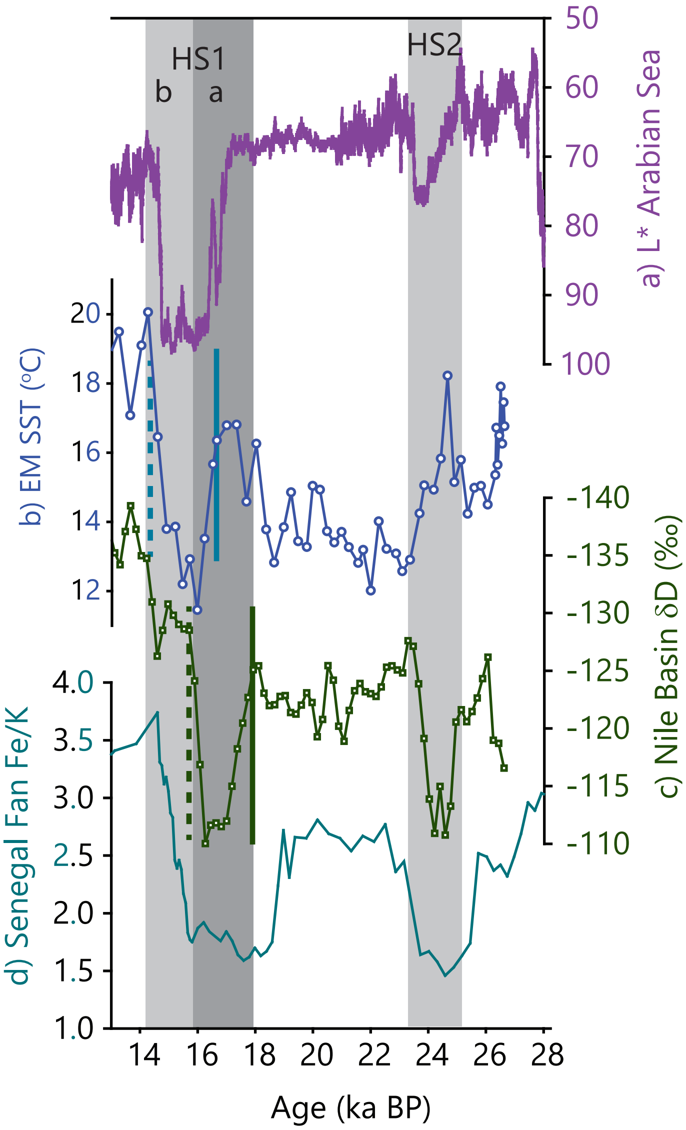

HS1
b
a
HS2
50
60
70
80
90
100
a) L* Arabian Sea
20
18
16
14
12
b) EM SST (ºC)
-140
-135
-130
-125
-120
-115
-110
c) Nile Basin δD (‰)
4.0
3.5
3.0
2.5
2.0
1.5
1.0
d) Senegal Fan Fe/K
14
16
18
20
22
24
26
28
Age (ka BP)

Figure 6

Supplementary Information: Hydroclimate variability in the Nile River Basin during the past 28,000 years

1. Figure 1 with full list of sites and references

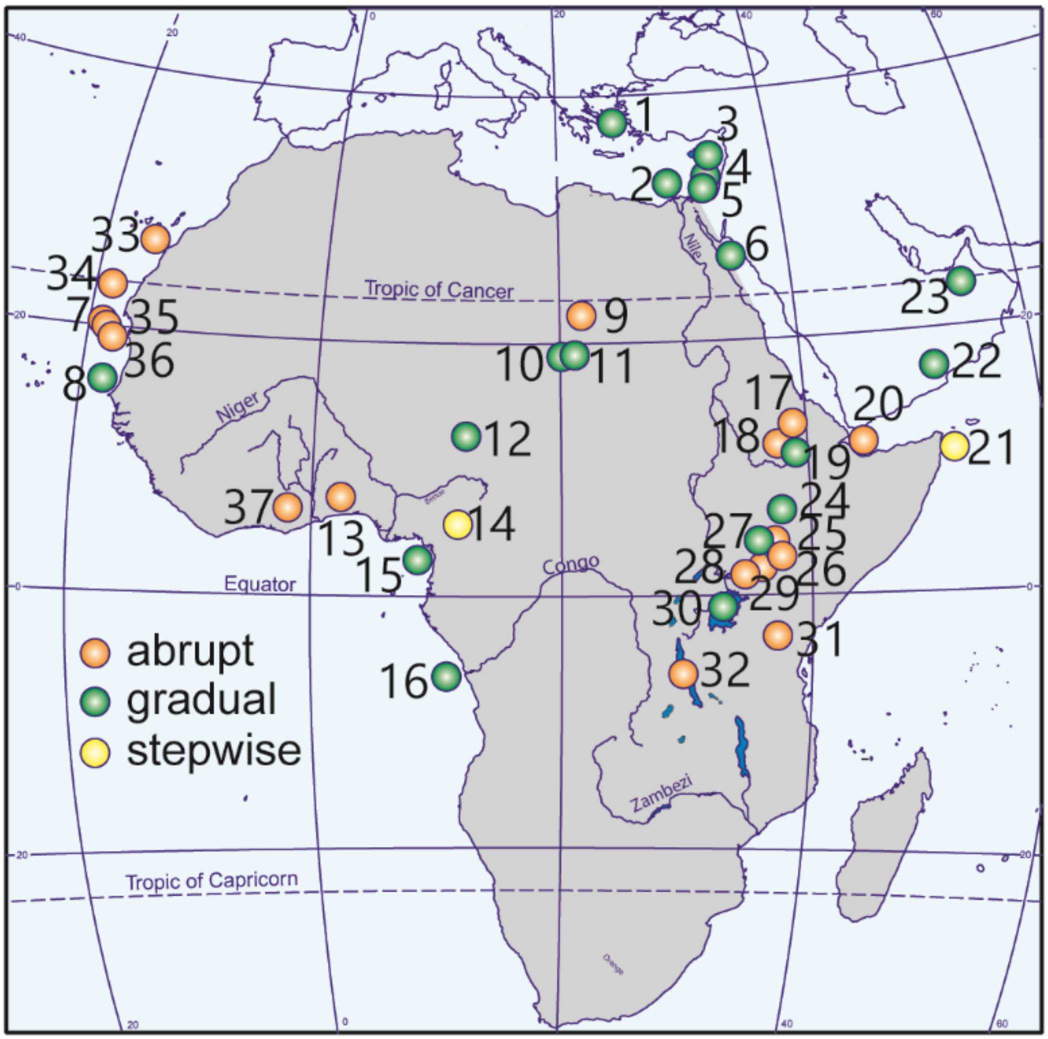

Figure 1 caption: In this version, the full site names and reference details are provided. The termination of the early Holocene Humid Period in North Africa. The colored circles indicate sites where the transition out of the African Humid Period is observed to be abrupt (orange), gradual (green) or stepwise (yellow). Note that the study locations depicted by the dots are approximate and in some cases have been shifted slightly where dots overlapped. The sites are as follows: 1. Agean Sea core SL143 [*Ehrmann et al.*, 2013]. 2. Nile deep-sea fan core P362/2-33 [*Blanchet et al.*, 2013]. 3. Eastern Mediterranean Sea core MD 9501 [*Box et al.*, 2011]. 4. Eastern Mediterranean Sea Core

SL112 [*Weldeab et al.*, 2014]. 5. Eastern Mediterranean Sea core 9509 [*Box et al.*, 2011]. 6. Red Sea core GeoB 5844-2 [*Arz et al.*, 2003]. 7. ODP Site 658C off Cap Blanc, Mauritania [*deMenocal et al.*, 2000]. 8. Core GeoB 9508-5, located near the mouth of the Senegal River. Note that two studies have been conducted on this core [*Mulitza et al.*, 2008; *Niedermeyer et al.*, 2010]. 9. The Gilf Kebir Plateau in southwest Egypt [*Linstädter and Kröpelin*, 2004]. 10. Lake Yoa in the Sahara [*Kröpelin et al.*, 2008]. 11. Lake Yoa in the Sahara [*Francus et al.*, 2013]. 12. Lake Chad core LT1 [*Amaral et al.*, 2013]. 13. Lac Sele in Southern Benin [*Salzmann and Hoelzmann*, 2005]. 14. Core M4 from Lake Mbalang in central Cameroon [*Vincens et al.*, 2010]. 15. Core MD03-2707 from the Gulf of Guinea [*Weldeab et al.*, 2007]. 16. Core GeoB 6518 from the vicinity of the Congo River outflow. Note that two studies have been conducted on this core [*Weijers et al.*, 2007; *Schefuß et al.*, 2005]. 17. Core 03AL3/2 from Lake Ashenge in Northern Ethiopia [*Marshall et al.*, 2009]. 18. Lake Tana core 03TL2 [*Marshall et al.*, 2011]. 19. Lake Tana core 03TL2 [*Costa et al.*, 2014]. 20. Gulf of Aden core P178-15P [*Tierney et al.*, 2013]. 21. Core 905 from the Arabian Sea, offshore Somalia [*Jung et al.*, 2004]. 22. Stalagmite Q5 from Qunf Cave in southern Oman [*Fleitmann et al.*, 2003]. 23. Stalagmites H5 and H12 from Hoti Cave in northern Oman [*Fleitmann et al.*, 2007]. 24. Core CB-01-09 from the Chew Bahir Basin in East African Rift Valley [*Foerster et al.*, 2012]. 25. The Mt. Porr strand plain along the southeastern shore of Lake Turkana [*Forman et al.*, 2014]. 26. Abandoned Holocene shorelines from the Lake Turkana basin, northern Kenya Rift [*Garcin et al.*, 2012]. 27. Cores LT84-2P and LT84-7P from the southern and northern basin of Lake Turkana [*Berke et al.*, 2012a]. 28. Suguta Valley lacustrine deposits [*Junginger et al.*, 2014]. 29. Lake Suguta, northern Kenya Rift [*Garcin et al.*, 2009]. 30. Lake Victoria core V95-1P [*Berke et al.*, 2012b]. 31. Lake Challa, located on the east slope of Mt. Kilimanjaro, Kenya [*Tierney et al.*, 2011]. 32. Lake Tanganyika cores NP04-KH04-3A-1K and NP04-KH04-4A-1K [*Tierney et al.*, 2008]. 33-36. Northwest African margin cores OC437-7GC37 (33), OC437-7GC49 (34), OC437-7GC66 (35) and OC437-7GC68 (36) [*McGee et al.*, 2013]. 37. Lake Bosumtwi ICDP drill core [*Shanahan et al*., 2015].

2. Influence of vegetation change on leaf wax deuterium isotopes

Following the approach of *Kuechler et al.* [2013], we use the $\delta^{13}C_{wax}$ values to estimate the percent C_4 vegetation shifts at site GeoB7702-3 along with published apparent fractionation factors of -123‰ for C_3 vegetation and -139‰ for C_4 vegetation [*Sachse et al.*, 2012]. We find that the maximum shift in δD_{wax} caused by vegetation changes is approximately 2‰ for the older portion of the record (Figure 2). Even considering the entire $\delta^{13}C_{wax}$ range of 4.1‰ in GeoB7702-3, the resulting shift in δD_{wax} of approximately 7‰ is minor in comparison to the large changes noted in the δD_{wax} record. Furthermore, the entire 0-28 ka BP Nile Basin δD_{wax} record displays similar trends to δD_{wax} records from the Congo Basin [*Schefuß et al.*, 2005], the Gulf of Aden [*Tierney et al.*, 2013] and Lake Tanganyika [*Tierney et al.*, 2008] (Fig. 5), sites located vast distances apart and characterized by different vegetation types [*White*, 1983], further confirming that vegetation shifts were not a main factor driving variability in δD_{wax}. Indeed, a recent study of $\delta^{13}C_{wax}$ and δD_{wax} in a transect of cores collected off the coast of western Africa concluded that vegetation changes (C_3 trees and C_4 grasses) exert only a minor influence on δD_{wax} in comparison to changes in the isotopic composition of precipitation [*Collins et al.*, 2013].

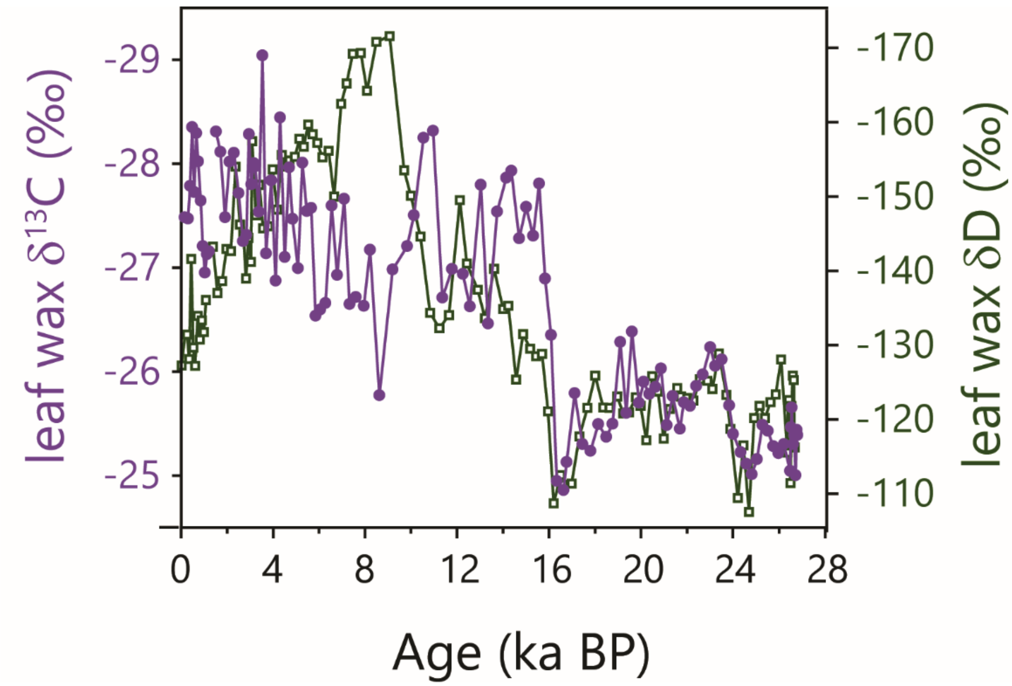

Figure 2 caption: Leaf wax $\delta^{13}C$ (purple circles) and δD (open green squares) values for core GeoB7702-3 plotted on top of each other for comparison.

Supplemental References:

Amaral, P., A. Vincens, J. Guiot, G. Buchet, P. Deschamps, J. Doumnang, and F. Sylvestre (2013), Palynological evidence for gradual vegetation and climate changes during the African Humid Period termination at 13°N from a Mega–Lake Chad sedimentary sequence, *Climate of the Past*, *9*(1), 223–241.

Arz, H. W., J. P¨atzold, P. J. Mu¨ller, and M. O. Moammar (2003), Influence of Northern Hemisphere climate and global sea level rise on the restricted Red Sea marine environment during termination I, *Paleoceanography*, *18*(2).

Berke, M. A., T. C. Johnson, J. P. Werne, S. Schouten, and J. S. Sinninghe Damsté (2012a), A mid-Holocene thermal maximum at the end of the African Humid Period, *Earth and Planetary Science Letters*, *351352*(0), 95 – 104, doi:http://dx.doi.org/10.1016/j.epsl.2012.07.008.

Berke, M. A., T. C. Johnson, J. P. Werne, K. Grice, S. Schouten, and J. S. Sinninghe Damsté (2012b), Molecular records of climate variability and vegetation response since the Late Pleistocene in the Lake Victoria basin, East Africa, *Quaternary Science Reviews*, *55*, 59–74.

Blanchet, C. L., R. Tjallingii, M. Frank, J. Lorenzen, A. Reitz, K. Brown, T. Feseker, and W. Bru¨ckmann (2013), High-and low-latitude forcing of the Nile River regime during the Holocene inferred from laminated sediments of the Nile deep-sea fan, *Earth and Planetary Science Letters*, *364*, 98–110.

Box, M., M. Krom, R. Cliff, M. Bar-Matthews, A. Almogi-Labin, A. Ayalon, and M. Paterne (2011), Response of the Nile and its catchment to millennial-scale climatic change since the LGM from Sr isotopes and major elements of East Mediterranean sediments, *Quaternary Science Reviews*, *30*(3), 431–442.

Collins, J. A., E. Schefuß, S. Mulitza, M. Prange, M. Werner, T. Tharammal, A. Paul, and G. Wefer (2013), Estimating the hydrogen isotopic composition of past precipitation using leaf-waxes from western Africa, *Quaternary Science Reviews*, *65*, 88–101.

Costa, K., J. Russell, B. Konecky, and H. Lamb (2014), Isotopic reconstruction of the African Humid Period and Congo Air Boundary migration at Lake Tana, Ethiopia, *Quaternary Science Reviews*, *83*(0), 58 – 67, doi:http://dx.doi.org/10.1016/j.quascirev.2013.10.031.

deMenocal, P., J. Ortiz, T. Guilderson, J. Adkins, M. Sarnthein, L. Baker, and M. Yarusinsky (2000), Abrupt onset and termination of the African Humid Period:: rapid climate responses to gradual insolation forcing, *Quaternary Science Reviews*, *19*(15), 347 – 361, doi:http://dx.doi.org/ 10.1016/S0277-3791(99)00081-5.

Ehrmann, W., M. Seidel, and G. Schmiedl (2013), Dynamics of Late Quaternary North African humid periods documented in the clay mineral record of central Aegean Sea sediments, *Global and Planetary Change*, *107*(0), 186 – 195, doi:http://dx.doi.org/10.1016/j.gloplacha.2013.05.010.

Fleitmann, D., S. J. Burns, M. Mudelsee, U. Neff, J. Kramers, A. Mangini, and A. Matter (2003), Holocene forcing of the Indian monsoon recorded in a stalagmite from southern Oman, *Science*, *300*(5626), 1737–1739.

Fleitmann, D., S. J. Burns, A. Mangini, M. Mudelsee, J. Kramers, I. Villa, U. Neff, A. A. Al-Subbary, A. Buettner, D. Hippler, et al. (2007), Holocene ITCZ and Indian monsoon dynamics recorded in stalagmites from Oman and Yemen (Socotra), *Quaternary Science Reviews*, *26*(1), 170–188.

Foerster, V., A. Junginger, O. Langkamp, T. Gebru, A. Asrat, M. Umer, H. F. Lamb, V. Wennrich, J. Rethemeyer, N. Nowaczyk, et al. (2012), Climatic change recorded in the sediments of the Chew Bahir basin, southern Ethiopia, during the last 45,000 years, *Quaternary International*, *274*, 25–37.

Forman, S. L., D. K. Wright, and C. Bloszies (2014), Variations in water level for Lake Turkana in the past 8500 years near Mt. Porr, Kenya and the transition from the African Humid Period to Holocene aridity, *Quaternary Science Reviews*, *97*, 84–101.

Francus, P., H. Von Suchodoletz, M. Dietze, R. V. Donner, F. Bouchard, A.-J. Roy, M. Fagot, D. Verschuren, and S. Kröpelin (2013), Varved sediments of Lake Yoa (Ounianga Kebir, Chad) reveal progressive drying of the Sahara during the last 6100 years, *Sedimentology*, *60*(4), 911–934.

Garcin, Y., A. Junginger, D. Melnick, D. O. Olago, M. R. Strecker, and M. H. Trauth (2009), Late Pleistocene–Holocene rise and collapse of Lake Suguta, northern Kenya Rift, *Quaternary Science Reviews*, *28*(9), 911–925.

Garcin, Y., D. Melnick, M. R. Strecker, D. Olago, and J.-J. Tiercelin (2012), East African mid-Holocene wetdry transition recorded in palaeoshorelines of Lake Turkana, northern Kenya Rift, *Earth and Planetary Science Letters*, *331332*(0), 322 – 334, doi:http://dx.doi.org/10.1016/j. epsl.2012.03.016.

Jung, S., G. Davies, G. Ganssen, and D. Kroon (2004), Stepwise Holocene aridification in NE Africa deduced from dust-borne radiogenic isotope records, *Earth and Planetary Science Letters*, *221*(1), 27–37.

Junginger, A., S. Roller, L. A. Olaka, and M. H. Trauth (2014), The effects of solar irradiation changes on the migration of the Congo Air Boundary and water levels of paleo-Lake Suguta, Northern Kenya Rift, during the African Humid Period (15–5 ka BP), *Palaeogeography, Palaeoclimatology, Palaeoecology*, *396*(0), 1 – 16, doi:http://dx.doi.org/10.1016/j. palaeo.2013.12.007.

Kröpelin, S., D. Verschuren, A.-M. L´ezine, H. Eggermont, C. Cocquyt, P. Francus, J.-P. Cazet, M. Fagot, B. Rumes, J. Russell, et al. (2008), Climate-driven ecosystem succession in the Sahara: the past 6000 years, *Science*, *320*(5877), 765–768.

Kuechler, R., E. Schefuß, B. Beckmann, L. Dupont, and G. Wefer (2013), Nw African hydrology and vegetation during the Last Glacial cycle reflected in plant-wax-specific hydrogen and carbon isotopes, *Quaternary Science Reviews*, *82*, 56–67.

Linstädter, J., and S. Kröpelin (2004), Wadi Bakht revisited: Holocene climate change and prehistoric occupation in the Gilf Kebir region of the Eastern Sahara, SW Egypt, *Geoarchaeology*, *19*(8), 753–778.

McGee, D., P. deMenocal, G. Winckler, J. Stuut, and L. Bradtmiller (2013), The magnitude, timing and abruptness of changes in North African dust deposition over the last 20,000 yr, Earth and Planetary Science Letters, 371, 163–176.

Marshall, M. H., H. F. Lamb, S. J. Davies, M. J. Leng, Z. Kubsa, M. Umer, and C. Bryant (2009), Climatic change in northern Ethiopia during the past 17,000 years: a diatom and stable isotope record from Lake Ashenge, *Palaeogeography, Palaeoclimatology, Palaeoecology*, *279*(1), 114–127.

Marshall, M. H., H. F. Lamb, D. Huws, S. J. Davies, R. Bates, J. Bloemendal, J. Boyle, M. J. Leng, M. Umer, and C. Bryant (2011), Late Pleistocene and Holocene drought events at Lake Tana, the source of the Blue Nile, *Global and Planetary Change*, *78*(3), 147–161.

Mulitza, S., M. Prange, J.-B. Stuut, M. Zabel, T. von Dobeneck, A. C. Itambi, J. Nizou, M. Schulz, and G. Wefer (2008), Sahel megadroughts triggered by glacial slowdowns of Atlantic meridional overturning, *Paleoceanography*, *23*(4).

Nicholson, S. E. (2011), *Dryland climatology*, Cambridge University Press.

Niedermeyer, E. M., E. Schefuß, A. L. Sessions, S. Mulitza, G. Mollenhauer, M. Schulz, and G. Wefer (2010), Orbital-and millennial-scale changes in the hydrologic cycle and vegetation in the western African sahel: insights from individual plant wax δD_{wax} and $\delta^{13}C_{wax}$, *Quaternary Science Reviews*, *29*(23), 2996–3005.

Sachse, D., I. Billault, G. J. Bowen, Y. Chikaraishi, T. E. Dawson, S. J. Feakins, K. H. Freeman, C. R. Magill, F. A. McInerney, M. T. Van der Meer, et al. (2012), Molecular paleohydrology: interpreting the hydrogen-isotopic composition of lipid biomarkers from photosynthesizing organisms, *Annu. Rev. Earth Planet. Sci*, *40*, 221–249.

Salzmann, U., and P. Hoelzmann (2005), The Dahomey Gap: an abrupt climatically induced rain forest fragmentation in West Africa during the late Holocene, *The Holocene*, *15*(2), 190–199.
Schefuß, E., S. Schouten, and R. R. Schneider (2005), Climatic controls on central African hydrology during the past 20,000 years, *Nature*, *437*(7061), 1003–1006.
Tierney, J. E., J. M. Russell, Y. Huang, J. S. Sinninghe Damsté, E. C. Hopmans, and A. S. Cohen (2008), Northern hemisphere controls on tropical southeast African climate during the past 60,000 years, *Science*, *322*(5899), 252–255.
Tierney, J. E., J. M. Russell, J. S. Sinninghe Damsté, Y. Huang, and D. Verschuren (2011), Late Quaternary behavior of the East African monsoon and the importance of the Congo Air Boundary, *Quaternary Science Reviews*, *30*(78), 798 – 807, doi:http://dx.doi.org/10.1016/j.quascirev. 2011.01.017.
Tierney, J. E., et al. (2013), Abrupt shifts in Horn of Africa hydroclimate since the Last Glacial Maximum, *Science*, *342*(6160), 843–846.
Vincens, A., G. Buchet, M. Servant, et al. (2010), Vegetation response to the "African Humid Period" termination in Central Cameroon (7°N)– new pollen insight from Lake Mbalang, *Climate of the Past*, *6*(3), 281– 294.
Weijers, J. W., E. Schefuß, S. Schouten, and J. S. Sinninghe Damsté (2007), Coupled thermal and hydrological evolution of tropical Africa over the last deglaciation, *Science*, *315*(5819), 1701–1704.
Weldeab, S., D. W. Lea, R. R. Schneider, and N. Andersen (2007), Centennial scale climate instabilities in a wet early Holocene West African monsoon, *Geophysical Research Letters*, *34*(24).
Weldeab, S., V. Menke, and G. Schmiedl (2014), The pace of East African monsoon evolution during the Holocene, *Geophysical Research Letters*, *41*(5), 1724–1732.
White, F. (1983), *The vegetation of Africa. A descriptive memoir to accompany the Unesco/AETFAT/UNSO vegetation map of Africa*, Natural Resources Research 20, 356 pp., UNESCO, Paris.